Skeletal Muscle Proteostasis Promotes Central Nervous System Rejuvenation and Reduces Neuroinflammation during Aging and Neurodegenerative Disease

Ian Matthews [1]

Allison Birnbaum [1]

Anastasia Gromova [2,3]

Kristen Coutinho [1]

Megan McGraw [1]

Dalton Patterson [1]

Macy T. Banks [1]

Amber Nobles [1]

Nhat Nguyen [3]

Helen C. Miranda [9-11]

Albert R. La Spada [3,12]

Constanza J. Cortes [1,4-8](corresponding author)

[1] Department of Cell, Developmental and Integrative Biology, [2] Biomedical Sciences Graduate Program, University of California, San Diego [3] Department of Pathology and Laboratory Medicine, University of California, Irvine [4] UAB Center for Exercise Medicine, [5] UAB Nathan Shock Center, [6] UAB Alzheimer's Disease Center, [7] UAB Center for Neurodegeneration and Experimental Therapeutics, [8] University of Alabama at Birmingham, [9] Department of Genetics and Genome Sciences, School of Medicine, Case Western University, [10] Department of Neurosciences, School of Medicine, Case Western Reserve University, [11] RNA Center, School of Medicine, Case Western Reserve University, [12] Department of Neurology and Department of Biological Chemistry, UCI Institute for Neurotherapeutics, University of California, Irvine

Funding: NIH RF1 AG057264 (CJC and ALS), NIH R03 AG063215 (CJC), University of Washington Nathan Shock Center Pilot Grant (CJC), NIH R35 122140 (ALS).

Acknowledgements: we thank members of the lab past and present for their helpful contributions

ABSTRACT

Skeletal muscle has recently arisen as a novel regulator of Central Nervous System (CNS) function and aging, secreting bioactive molecules known as myokines with proteostasis and metabolism-modifying functions in targeted tissues, including the CNS. Here we report the generation of a novel transgenic mouse with enhanced skeletal muscle proteostasis via moderate overexpression of master regulator of proteostasis and lysosomal function Transcription Factor E-B. We have discovered that the resulting enhanced muscle proteostasis function significantly ameliorates proteotoxicity, reduces neuroinflammation and promotes transcriptional remodeling of the aging CNS, preserving cognition and memory in aging mice. Enhancing skeletal muscle proteostasis also reduces neuroinflammation and accumulation of tau-associated pathological hallmarks in a mouse model of tau pathology. Our results implicate maintenance of skeletal muscle proteostasis throughout aging to direct regulations of the aging CNS metabolism and function, and suggest that skeletal-muscle originating factors may act as novel therapeutic targets against age-associated neurodegenerative diseases.

INTRODUCTION

Aging is associated with an organism-wide progressive loss of tissue form and function, broadly characterized by the 'hallmarks of aging'[1]. In particular, the aging central nervous system (CNS)[1,2] exhibits a global loss in protein homeostasis (proteostasis), impaired neuroplasticity and resilience, and an increase in neuroinflammation[2,3]. These alterations are believed to render the aging CNS vulnerable to age-associated dysfunction and the development of neurodegenerative disease[2]. A central player in proteostasis function is macroautophagy (hereafter referred to as autophagy), which degrades and recycles intracellular material such as dysfunctional mitochondria, protein aggregates, and other large subcellular components too large to be processed through the proteasome. Autophagy activity steadily declines with age[4], leading to a chronic accumulation of damaged macromolecules and organelles in aging tissues[4] and contributing to the onset of age-associated diseases[1,4]. In concordance with this, genetic disruption of autophagy in specific cell types is sufficient to drive cellular and biochemical hallmarks of aging in young tissues, including accumulation of protein aggregates[5,6], mitochondrial dysfunction[7] and compromised metabolic signaling[7-9]. Autophagy dysfunction has thus been proposed to act as a primary regulator of biological aging[1,4]. Consistent with this hypothesis, many well-known geroprotective interventions appear to work through the promotion of autophagy function[4]. Indeed, studies have shown that maintenance of global autophagy via genetic[10-12], behavioral[13] and pharmacological[14,15] manipulation extends lifespan and/or healthspan in murine and primate models. Autophagy activation *in vivo* also delays the development of age-associated metabolic phenotypes[7,13,16] and preserves motor function during aging[11]. Taken together, these results position autophagy as an excellent target for therapeutic development to prevent age-associated CNS functional decline.

Elegant genetic studies on non-vertebrate models have recently revealed the existence of transcriptional protein quality control feedback between tissues, i.e. the cell-non autonomous control of organismal proteostasis[17-21]. In particular, manipulation of skeletal muscle protein quality control pathways yields important benefits to the CNS by activating proteostasis and protecting against the accumulation of aggregation-prone neurodegenerative disease proteins in the brain and the retina[18,21,22]. Although the mechanisms responsible for these benefits remain poorly understood, some of these effects are mediated by secreted factors that move through the invertebrate circulation[18,20,22]. Indeed, increasing evidence implicates circulating factors in the blood as potent regulators of mammalian CNS aging and metabolism[23-26]. For example, exposure to a young plasma environment (either through heterochronic parabiosis or plasma

transfers) can rescue function in the aging CNS[25,27] by decreasing neuroinflammation[28] and enhancing neurogenesis[23]. Studies have further demonstrated that increasing the circulating levels of these individual factors in peripheral circulation is sufficient to rejuvenate the aged CNS[25,29,30], supporting the existence of geroprotective circulating factors with CNS targeting effects. Although the source and identity of these neuroprotective circulating cytokines are unclear, several of them are expressed in, and can be secreted from, skeletal muscle[18,31-33]. Indeed, skeletal muscle acts as an endocrine organ secreting a myriad of bioactive factors collectively known as myokines that induce metabolic changes in distant tissues like liver[34], adipose tissue[35], and even the CNS[32]. Interestingly, skeletal muscle function has also arisen as a key predictor for phenotypic and clinical outcomes in age-associated neurodegenerative diseases, including Alzheimer's Disease (AD) and Parkinson's Disease (PD)[36,37]. Thus, this muscle-to-brain signaling axis has been proposed to have important implications for CNS aging and age-associated neurodegenerative disease[32,38,39]. Consistent with this hypothesis, we were the first to uncover a novel mechanistic basis for motor neuron disease in the polyglutamine disease spinal and bulbar muscular atrophy (SBMA), where disruption of skeletal muscle autophagy[40] initiates the pathogenic cascade that culminates in neuronal toxicity and death[41,42]. Altogether, this suggests that maintenance of skeletal muscle proteostasis may promote neurotrophic signaling in the aging brain, thus providing positive systemic benefits against age-associated CNS decline.

Skeletal muscle autophagy is regulated in part by the basic Helix Loop Transcription Factor E-B (TFEB), a master regulator of a novel signaling axis that integrates cellular metabolism and autophagy[43-45]. TFEB expression and function are strongly induced in skeletal muscle during low nutrient conditions[16] and after exercise[7], suggesting that TFEB signaling is engaged in skeletal muscle in response to interventions with documented neuroprotective effects on the aging[46,47] and neurodegenerative disease-afflicted CNS[47-50]. Here we report the generation of a novel transgenic mouse with enhanced muscle proteostasis via moderate overexpression of TFEB. We have discovered that the resulting enhanced skeletal muscle proteostasis function can significantly ameliorate proteotoxicity, reduce neuroinflammation and promote transcriptional remodeling of the aging CNS, preserving cognition/memory in aging mice. Enhancing skeletal muscle proteostasis also reduced accumulation of tau-associated pathological hallmarks and activation of astrocytes and microglia in a mouse model of tau pathology and was accompanied by increased secretion of CNS-targeting circulating factors from skeletal muscle. Our results implicate maintenance of skeletal muscle proteostasis throughout aging to direct regulations of

the aging CNS metabolism and function, and suggest that skeletal-muscle originating factors may act as novel therapeutic targets against age-associated neurodegenerative diseases.

RESULTS

TFEB Overexpression Activates Proteostasis-Related and Metabolism-Associated Networks in Skeletal Muscle

We derived a novel line of conditional transgenic mice carrying the β-actin promoter in combination with the CMV enhancer (CAGGS) and with a floxed 3x-FLAG-eGFP STOP cassette placed just 5' to a 3x-FLAG-human *Tcfeb* transgene ("fxSTOPTFEB" mice), allowing for tissue-specific expression of TFEB in the presence of Cre-recombinase (**Figure 1a**). To drive expression of the TFEB transgene specifically in skeletal muscle, we crossed fxSTOP-TFEB mice with Human Skeletal Actin (HSA)-Cre mice to achieve widespread expression of Cre-recombinase in cells of the myogenic lineage[51]. The resulting cTFEB;HSACre bigenic mice exhibited muscle-specific expression of 3x-FLAG-TFEB (**Figure 1b**). Indeed, we detected significant transcriptional increases in *Tcfeb* in skeletal muscle RNA lysates from young (6 months) and aged (24 months) cTFEB;HSACre transgenic mice compared to their littermate controls (**Supplementary Figure 3a-b**). We also confirmed myonuclear expression of TFEB in cTFEB;HSA-Cre muscle by immunohistochemistry, which revealed FLAG-positive immunostaining in the myofiber periphery (**Supplementary Figure 1b**).

We confirmed TFEB overexpression exclusively in skeletal muscle by multiple approaches. First, we did not detect exogenous expression of 3x-FLAG-TFEB in other highly metabolic tissues, including brown adipose tissue (**Supplementary Figure 2a),** liver **(Supplementary Figure 2b)** and the CNS **(Supplementary Figure 3).** Indeed, at all ages examined, we detected no differences in *Tcfeb* transcription in hippocampal lysates regardless of their genotype **(Supplementary Figure 3a-b)**. Consistent with these findings, we also did not detect expression of exogenous 3x-FLAG-TFEB in hemibrain protein lysates **(Supplementary Figure 3c).** We also confirmed robust activation of a red fluorescent protein reporter in skeletal muscle of TdTomato Ai9;HSA-Cre transgenic mice, which express robust tdTomato fluorescence following Cre-mediated recombination (**Supplementary Figure 1a**)[52]. Notably, there was no detectable TdTomato fluorescence in the CNS **(Supplementary Figure 3d)**, including the hippocampus (**Supplementary Figure 3d, insets),** of the same individuals, consistent with the muscle-restricted specificity of this Cre-loxP-ON approach. Overall, this data confirm previous

reports of striated muscle-specific Cre-mediated recombination using the HSA-Cre transgenic line[51], and demonstrate expression of exogenous *Tcfeb* only in skeletal muscle of cTFEB;HSACre transgenic mice.

TFEB directly regulates transcription of multiple lysosomal and autophagy-associated genes [43,45], promoting lysosomal function and autophagy activation in vivo[7,16] and in vitro[43,45]. We confirmed functional activation of TFEB-dependent transcription in cTFEB:HSA-Cre bigenic muscle, using our previously reported TFEB-responsive muscle gene targets[40] including *Lamp1* (an essential lysosomal structural protein), *Ctsd* (Cathepsin D, a lysosomal protease) and *Atg5* (a key regulator of autophagy initiation) (**Supplementary Figure 4a**). Immunoblotting studies also revealed significant increases of TFEB transcriptional targets at the protein level, including LAMP1 and CTSD (**Supplementary Figure 4b**). These findings confirm physiologically significant increases in TFEB- expression and TFEB-dependent transcription in skeletal muscle of cTFEB:HSA-Cre mice.

To examine the overall changes in the skeletal muscle protein landscape in response to TFEB overexpression, as well as any differences in protein expression profiles associated with aging, we performed proteome profiling of young and aged, control and cTFEB;HSACre quadriceps skeletal muscle. Differential abundance analysis of species revealed around 1000 proteins associated with TFEB expression in young (6-month-old) skeletal muscle (**Figure 1c**). Of these, 650 (65%) were significantly overrepresented and 35% (350) were underrepresented with TFEB-overexpression. At 18 months of age, a time point where age-associated dysfunction is prevalent in murine skeletal muscle [53], we detected around 400 differentially expressed proteins in TFEB-expressing skeletal muscle (**Figure 1d**). Of these, 83% (250) were significantly enriched and 17% (50) were significantly decreased in cTFEB;HSACre transgenic muscle. Importantly, at both ages examined, TFEB remained among the top 5 most highly expressed proteins (**Figure 1c-d**), confirming maintenance of exogenous skeletal muscle TFEB expression across ages.

To visualize the key networks of proteins associated with TFEB-overexpression, we performed a functional enrichment analysis on all overexpressed proteins using the STRING protein-protein interaction network[54] (**Figure 1e and Supplementary Figure 4**). Using TFEB as our 'bait' for functional connectivity nodes, we identified two clear interaction networks: one associated with lysosomal biogenesis and function (**Figure 1e, blue**) and a second one associated with key skeletal muscle proteostasis and metabolic signaling pathways, including

mTOR, AKT and GSK3β (**Figure 1e, green**). Both of these nodes are key elements of the CLEAR signaling network controlled by TFEB-mediated transcription[44,45], were previously reported to be transcriptionally elevated in skeletal muscle after TFEB overexpression[7], and are central regulators of age-associated signaling[1].

Next, we grouped all overrepresented proteins using Kyoto Encyclopedia of Genes and Genomes (KEGG) enrichment analysis. We detected multiple central proteostasis categories heavily overrepresented in TFEB-overexpressing skeletal muscle, including Hypoxia-inducible factor 1 (HIF-1) signaling (such as hexokinase 2, Pyruvate Dehydrogenase, Ribosomal Protein S6 Kinase B2 and Lactate Dehydrogenase B) and proteasome and autophagy/lysosomal function categories (including cathepsin B (CTSB), D and K, mTOR, BNIP3 and LAMP1) (**Figure 1f)**, consistent with our targeted immunoblot studies (**Supplementary Figure 4**). Importantly, this enrichment in proteostasis categories and TFEB-regulated nodes of signaling was maintained in aging skeletal muscle (**Figure 1f and Supplementary Figure 5**).

TFEB overexpression has been reported to reactivate declining proteostasis associated with age- or disease-associated impaired lysosomal function[40,55,56]. We wondered if the enrichment in proteostasis pathways and proteostasis signaling observed in aged skeletal muscle with TFEB-overexpression would result in functional outcomes reflective of proteostasis maintenance. Consistent with this hypothesis, analysis of autophagy marker LC3, which is cleaved and post-translationally modified into its mature form (LC3-II) upon autophagy induction[57], revealed a significant increase in LC3-II:LC3-I ratio in quadriceps muscle of 12 month-old cTFEB:HSA-Cre mice, suggesting increased accumulation of autophagosomes (**Supplementary Figure 6a**). Another approach to examining the age-associated decline in proteostasis is the examination of poly-ubiquitinated and P62-labeled aggregates, usually representing cytoplasmic accumulations of damaged proteins[4]. We found a marked accumulation of P62/SQSTM1 and ubiquitin-positive aggregates of varying size in middle-aged control skeletal muscle (**Supplementary Figure 6b, top**), indicating a progressive increase in protein damage and a decrease in the turnover of skeletal muscle proteins [1,21,58]. Strikingly, these features were nearly absent in skeletal muscle sections from age- and littermate-matched cTFEB:HSA-Cre mice (**Supplementary Figure 6b, bottom**). This suggests that in addition to activating lysosomal biology and function, expression of TFEB in skeletal muscle results in functional activation of autophagy, reducing the accumulation of age-associated protein inclusions.

Additional functional categories enriched in our proteomics analysis related to cellular metabolism and mitochondrial function, including thermogenesis, oxidative phosphorylation and fatty acid metabolism. Notably, several signaling pathways shown to decline during aging, including Insulin-IGF1-signaling (IIS) and AMPK signaling[1], were significantly enriched in cTFEB;HSACre transgenic muscle (**Figure 1f**). We also detected multiple hits for amino acid metabolism pathways, such as catabolism of branched-chain amino acids (BCAAs), including valine, leucine and isoleucine metabolism. These changes were still evident in our aged cohorts (**Figure 1f**), suggesting preservation of multiple key hallmarks of aging (i.e. proteostasis, metabolism, and mitochondrial function) via maintenance of TFEB-associated signaling in aging skeletal muscle. In agreement with this, analysis of skeletal muscle of 12-month-old control mice showed marked accumulation of age-associated histopathological markers, including fiber decompaction, intrafibrillary myonuclei and multilamellar structure accumulation (**Supplementary Figure 7a, top**). Remarkably, these features were nearly absent in skeletal muscle sections from age- and littermate-matched cTFEB:HSA-Cre mice (**Supplementary Figure 7a, bottom**). Instead, aging cTFEB;HSACre muscle retained compact fiber organization and perifibrillar myonuclei and did not exhibit any multilammelar structures. Furthermore, we also detected reduced expression of muscle stress factor *Mstn* (myostatin) [59] (**Supplementary Figure 7b**) and increased expression of metabolic modulator *Fndc5* [59] in aged cTFEB;HSACre skeletal muscle (**Supplementary Figure 7c**). Our results suggest maintenance of functional proteostasis via TFEB overexpression throughout aging has multiple geroprotective benefits in skeletal muscle.

The skeletal muscle 'secretome' (the totality of released organic and inorganic molecules released from muscle resident cells) is highly dynamic, responding to physiological and pathophysiological stimuli [59,60] and potentially also changing with age [59]. To directly examine any changes to the skeletal muscle protein-based secretome associated with TFEB-overexpression, we pursued additional *in silico* analysis on our proteomics cohorts to identify unique age- and genotype-associated signatures of potentially secreted proteins[61] differentially expressed in cTFEB;HSACre skeletal muscle. Using the Vertebrate Secretome Database (VerSeDa)[61], we identified multiple proteins with predicted secreted profiles to be enriched in young and aged TFEB-expressing skeletal muscle (**Figure 2a**). Some secreted proteins exhibited upregulation (e.g., nucleobindin-1, angiopoietin-related protein 1) or down-regulation (collagen alpha-1 (I) chain), only in young cTFEB;HSACre muscle. Others remained up-regulated at both ages in cTFEB;HSACre-expressing muscle, (prosaposin and mammalian ependymin-related protein 1

and dehydrogenase/ reductase SDR family member 7C), highlighting the dynamic nature of the skeletal muscle 'secretome' throughout aging. CTSB, a previously documented muscle-originating secreted factor with known CNS-targeting effects[33] and a known target of TFEB-dependent transcription[45] was our top hit at both ages examined. We validated the predicted increase in *Ctsb* at the transcriptional level in a separate cohort of cTFEB;HSACre mice (**Figure 2c**). Interestingly, while we detected no significant differences in total or pro-enzyme levels of CTSB, we determined a specific increase in mature CTSB isoforms (**Figure 2b**). CTSB undergoes auto –proteolytic activation within the acidic environment of late endosomes/lysosomes, and mature CTSB is then secreted via lysosomal exocytosis. Consistent with this enrichment on potentially secreted CTSB isoforms, we detected significantly increased levels of circulating CTSB in the serum of cTFEB;HSACre mice (**Figure 2d**). Given the potent remodeling of the lysosomal network associated with activation of TFEB-mediated transcription [43-45], our data suggests that overexpression of TFEB in skeletal muscle drives increased expression and secretion of mature CTSB, a CNS targeting-factor, into circulation.

Skeletal Muscle Over-expression of TFEB decreases neuroinflammation markers and lipofuscin accumulation in the aged CNS.

One of the key drivers of age-associated cognitive decline is neuroinflammation[2], the chronic activation of glial cells towards pro-inflammatory phenotypes in the CNS. To examine the effect of increased peripheral proteostasis on the aging brain, we assessed the transcriptional and functional status of known inflammatory markers in the CNS of aged mice (20+ months), an age when global decreases in proteostasis and increases in pro-inflammatory signaling are detectable in most tissues[1,62], including the CNS[1,2].

Using standard immunostaining approaches to quantify cell shape and morphology, we did not detect any changes in microglia or astrocyte number, volume or ramification in the dentate gyrus of aged cTFEB;HSACre transgenic mice (**Supplemental Figure 8a-b**). However, total hippocampal mRNA levels of pro-inflammatory cytokines previously reported to mediate microglial responses to inflammation including *Ccl2* (also known as monocyte chemotactic protein-1, MCP1)[63] and *NFκB*[64] were significantly reduced in the hippocampus of aging female cTFEB;HSACre transgenic mice(**Figure 3a-b**). Interestingly, levels of *IL6* (interleukin 6) were significantly elevated in the same groups (**Figure 3c**). Although commonly considered a pro-inflammatory factor, IL-6 also appears to have seemingly contradictory neurotrophic effects in the CNS, increasing neurogenesis[65] and stimulating axon regeneration[66]. Consistent with these

findings, we also detected significantly higher levels of expression of *Bdnf* (Brain Derived Neurotrophic Factor) in hippocampal lysates from middle-aged (12-month old) female mice (**Figure 3d**). Overall, these results suggest a shift in the cytokine transcriptional landscape of the aging hippocampus with upregulated peripheral proteostasis to an overall reduction of anti-inflammatory phenotypes.

Accumulation of lipofuscin, a non-degradable intracellular auto-fluorescent polymer, becomes prominent in the aging brain, likely reflecting an age-associated decline in basal CNS autophagy[1]. We examined the clearance capabilities of the aging CNS by indirect immunofluorescence of lipofuscin granules in brain sections of aged (21-24 months-old) control and cTFEB;HSACre mice. While we detected striking lipofuscin granule accumulation in several brain regions of aged control mice, including the hippocampus, age- and littermate-matched cTFEB;HSACre mice revealed a decrease in lipofuscin deposition, particularly in the dentate gyrus of the female (**Figure 3e)** and male hippocampus (**Supplemental Figure 8c**). Taken together, these results indicate that maintenance of skeletal muscle proteostasis throughout aging reduces neuroinflammation and promotes maintenance of protein quality control in the aging hippocampus of cTFEB;HSACre transgenic mice. Importantly, this occurs in the absence of detectable exogenous TFEB expression in the CNS (**Supplemental Figure 3**), suggesting an independent mechanism of muscle-to-brain communication underlying the observed neuroprotective effects.

Improved Performance in Neurocognitive Testing of Aging cTFEB;HSACre Mice.

Geroprotective interventions that target the CNS can have direct effects on brain plasticity, with well-documented benefits on hippocampal-dependent cognitive functions[6,28,39,40]. Given the maintenance of proteostasis, reduction in neuroinflammation and increase in *Bdnf* expression observed in the aging hippocampi of cTFEB;HSACre transgenic mice, we pursued neurocognitive testing in aged (16-18 months-old) control and cTFEB;HSACre mice. First, we confirmed no difference in visual performance (optomotor test) (**Supplemental Figure 9a**), or motor activity (ambulatory, rearing or center activity, as well as distance traveled) (**Supplemental Figure 9b**) between aged control and cTFEB;HSACre cohorts. We then evaluated spatial learning and memory using the Barnes maze task, a hippocampal working memory test known to be sensitive to aging in mice. We documented significantly faster escape times (**Figure 3f)** and a significant decrease in the number of errors per trial (**Figure 3g**) in aged cTFEB;HSACre mice in comparison to controls. Indeed, by the last

trial, cTFEB;HSACre mice escaped the maze twice as quickly as control mice. In the novel object recognition task – an independent behavioral test of hippocampal recognition memory – we also found that aged cTFEB;HSACre mice exhibited a significantly greater number of contacts with the novel object compared to controls during the test phase (**Figure 3h**). Indeed, aged cTFEB;HSACre mice have a 15% higher preference for the novel object relative to their age-matched littermate controls (**Figure 3i**). Hence, these results provide exciting evidence for a pronounced improvement in neural function in the aging brain of cTFEB;HSACre mice with enhanced muscle proteostasis.

Neurotrophic Transcriptome Changes in the Hippocampi of cTFEB;HSACre transgenic mice.

To determine the molecular basis of the benefits of enhancing skeletal muscle proteostasis on the aging CNS, we performed unbiased transcriptome analysis on hippocampal RNAs isolated from young (6 months, adult) and aged (21+ months) mice. By this time point, aging animals have increased neuroinflammation (**Figure 3a**), have evident CNS proteostasis dysfunction (**Figure 3e**), and display deficits in cognitive function (**Figure 3g-i**), phenotypes that are significantly improved in cTFEB;HSACre mice.

Bulk RNA-Seq analysis of hippocampal RNA lysates revealed robust changes in gene expression in young cTFEB;HSACre transgenic mice compared to their age- and sex-matched littermate controls (**Figure 4 and Supplemental Figure 10**). We detected 1194 differentially expressed genes, (809 up-regulated and 385 down-regulated) in the hippocampus of young female mice with enhanced skeletal muscle proteostasis (**Figure 4a**). To identify specific neural signaling functions that could be contributing to the neuroprotective effects of enhancing skeletal muscle proteostasis, we performed GO Enrichment analysis of all differentially expressed genes. We found that key categories associated with synaptic function, including ion- and voltage-gated channel activity, as well as synapse and synaptic membrane categories, were significantly enriched in the hippocampus of female cTFEB;HSACre mice (**Figure 4c**). Enrichment analysis of differential gene expression (KEGG) revealed additional categories associated with neural function, including oxytocin signaling, cAMP signaling, Hippo signaling and gap junctions (**Figure 4e**). Furthermore, metabolic and functional pathway analysis (Reactome) of differentially expressed genes in the hippocampus after enhancing skeletal muscle proteostasis also identified key categories known to regulate cognitive plasticity,

including neuronal system, GPCR signaling, voltage gate potassium channels, and synaptic connectivity (Phase - -rapid depolarization and Phase 2 – plateau) (**Supplementary Figure 10**).

Consistent with our biochemical and functional findings suggesting increased neuroprotective benefits in cTFEB;HSACre transgenic mice (**Figure 3**), we found that these transcriptional changes modulating synaptic function-associated pathways are largely preserved in the aging hippocampus of cTFEB;HSACre transgenic mice (**Figure 4b,d,f**). Indeed, KEGG functional pathways enriched in the hippocampus of aging cTFEB;HSACre female mice included key categories associated with preservation of neuronal activity and cognitive function, including axon guidance, HIF-1 signaling, AMP signaling and PI3-Akt signaling (**Supplemental Figure 10**).

Analysis of the functional enrichment of top differentially expressed genes in the hippocampus of young male cTFEB;HSACre transgenic mice revealed a different pattern, (1797 differentially expressed genes, 928 up-regulated and 869 down-regulated), which associated mostly with multiple mitochondria or ribosomal/transcription targeting pathways (**Supplemental Figure 11**). This included mitochondrial respiratory chain, mitochondrial protein complexes, electron transport chain and ATP metabolic processes (**Supplemental Figure 11**). Non-sense mediated decay, metabolism of RNA and translation were amongst the top enriched metabolic pathways identified in male groups (**Supplemental Figure 12**). Consistent with this, KEGG analysis revealed the largest enriched functional pathways were ribosomes and oxidative phosphorylation (**Supplemental Figure 12**). We only detected 539 differentially expressed genes in the hippocampus of aged male cTFEB;HSACre transgenic mice (279 up-regulated, 261 down-regulated) (**Supplemental Figure 12**), with only mild significance on functional pathways. Altogether, these results suggest important transcriptional remodeling of the CNS in response to enhanced skeletal muscle proteostasis, that they reflect biological pathways essential for neuronal signaling and cognitive function and that these changes are preserved throughout aging.

Enhanced skeletal muscle proteostasis reduces accumulation of hyperphosphorylated tau and microglial activation in a mouse model of tau pathology.

To assess the potential neuroprotective effects of enhancing skeletal muscle proteostasis in the context of age-associated neurodegenerative disease pathologies, we derived cTFEB;HSACre transgenic mice in the MAPT P301S background. This is a well-known model of neurofibrillary

tangle toxicity, a hallmark of AD and related tauopathies[67], and is characterized by prominent hippocampal hyperphosphorylated tau accumulation and neuroinflammation, including microgliosis and astrocyte reactivity[67]. We confirmed muscle-restricted 3x-FLAG-TFEB overexpression in skeletal muscle lysates from MAPT P301S /cTFEB;HSACre mice but no 3x-FLAG-TFEB expression in their MAPT P301S littermates (**Supplemental Figure 13a**). We noted that at 9 months of age, when there is robust accumulation of hyperphosphorylated tau and neuroinflammation, and at the onset of behavioral phenotypes in this mouse model[67], we detected a significant reduction in the total fluorescence counts of hyperphosphorylated tau (AT8 phospho-tau antibody) in the dentate gyrus of cTFEB;HSACre;P301S mice compared with single transgenic P301S littermate controls (**Figure 5a**). Immunoblotting analysis confirmed a reduced phosphorylated tau to total tau ratio in whole hippocampal lysates of MAPT P301S transgenic mice with enhanced skeletal muscle proteostasis (**Supplemental Figure 13b**)**.** More so, there was also a significant reduction in the levels of 'intracellular tau' accumulating around hippocampal cell bodies (**Figure 5a, insets**), suggesting reduced accumulation of toxic tau species and aggregates[68] in the hippocampi of cTFEB;HSACre:P301S transgenic mice.

Glial cells (such as astrocytes and microglia), are key responders during neuroinflammation, and have been shown to undergo key morphological changes[69] including changes in ramification and cellular process complexity[69], which are believed to reflect reduced immune surveillance activity[70] and increased reactivity phenotypes [71]. Consistent with previous reports in this model[67,72], we confirmed significant increases in the number of GFAP-positive astrocytes, as well as increases in the volume of Iba1-positive microglia in the hippocampus of 9-month-old MAPT P301S mice (**Figure 5b**). Strikingly, we noted significant reductions in both of these pro-inflammatory associated morphometric parameters in the hippocampus of MAPT P301S;cTFEB;HSACre littermates (**Figure 5b and Supplemental Figure 13 c-d**), suggesting overall reduced neuroinflammation during symptomatic disease stages through activation of skeletal muscle proteostasis.

Enhancing Skeletal Muscle Proteostasis Promotes Neurotrophic Signaling and Reduces Hippocampal Neuroinflammation in MAPT P301S Transgenic Mice.

To gain more precise insights into neurodegenerative disease-relevant transcriptional changes in the hippocampus of MAPT P301S;cTFEB;HSACre mice, we used the Nanostring nCounter® AD panel. This platform directly assesses the expression of 770 genes curated from human and pre-clinical models of AD and robustly captures disease-relevant signatures and their

modifications after pre-clinical interventions[73]. Using this approach, we found a total of 79 differentially expressed genes in MAPT P301S;cTFEB;HSACre hippocampi compared to their littermate MAPT P301S+ controls (**Figure 6a-b**). Interestingly, most differentially regulated genes were downregulated (76 of 79), consistent with their identity as transcriptional drivers of disease[73]. Many of these transcripts are associated with microglial activation (including *Rhoc, Bcar3 and Alcam*), markers of neuronal function (*Gdap1l1),* phospholipid remodeling (*Ano6*), growth factor signaling (*Vgf*), endothelial cell migration and matrix adhesion (*Rras*) and guanine nucleotide exchange factors (*Dock3*). Interestingly, multiple down-regulated genes were associated with novel variants and loci associated with increased polygenic neurodegenerative disease risk (*Prkd3*[74]*, Bcar3*[75]*, Nfia*[76]*, Elovl7*[77]*)* as well as predictors of the rate of cognitive decline in AD (*Hecw1*[78]). Expression of *Arhgdib,* recently identified as a potential novel biomarker for tau neurofibrillary tangle accumulation and neuropathological Braak stage in human entorhinal cortex[79], was also significantly reduced. Similarly, *Pbxip1,* another significantly downregulated marker, has been found to be associated with phosphorylated-tau and $A\beta_{1–40}$ levels in the human temporal cortex[80]. Additional transcriptional reductions of significance include genes of unknown function but classified as transcriptional identifiers of AD progression *(Ptprn, Cpne2, Eri2)*[73]. Functional annotation of the differentially expressed co-expression/functional clusters revealed significant reductions in the nCounter microglial activation module (**Figure 6c**) in the hippocampi of 9 month old female MAPT P301S cTFEB;HSACre mice compared with P301S littermates, consistent with increased neuroprotection and reduced neuroinflammation in the hippocampus (**Figure 5**). Although no other functional clusters displayed statistically significant differences, multiple categories displayed interesting trends, suggesting a general modification of AD-associated transcriptional profile in the hippocampus in response to enhanced muscle proteostasis. This included changes in lipid metabolism (**Figure 6d**) and trophic factors (**Figure 6e**) as well as transcription/splicing, axon guidance and others (**Supplementary Figure 14**). Similar to what we observed in our healthy aging groups (**Figure 3d**), we also confirmed re-activation of neurotrophic signaling in the hippocampus of MAPT P301S cTFEB;HSACre symptomatic mice, measured by the corrections of declining expression levels of neurotrophic factors *Bdnf* and *Fndc5* (**Figure 6f-g**)[38,81]. These provocative results suggest that enhanced skeletal muscle proteostasis modifies the accumulation of pathogenic tau isoforms and reduces neuroinflammation in the hippocampus of P301S mice via transcriptional remodeling and activation of neurotrophic signaling in the CNS.

DISCUSSION

Skeletal muscle comprises roughly 40% of the total body mass in a healthy young adult human and is highly susceptible to age-associated proteostatic decline[58,82]. Muscle autophagy facilitates metabolic reprogramming and mitochondrial quality control during conditions of high metabolic demand[16,83,84] and is also required to maintain muscle health and muscle mass[85,86 87]. Skeletal muscle health has been linked to multiple chronic age-associated conditions, including diabetes[88], cardiovascular disease[89] and, more recently, neurodegenerative diseases[36,37,39]. In agreement with this, muscle-originating circulating factors (myokines) appear to play central roles in regulating CNS health and function. For example, Amyrel amylase, a skeletal muscle secreted protein with maltose producing function, was recently identified as a key proteostasis stress-induced myokine with CNS targeting effects in *Drosophila Melanogaster*[18]. Consistent with our own findings here, muscle-specific *amyrel* overexpression improves proteostasis and prevents neurodegeneration induced by aggregation-prone disease-associated pathogenic proteins in the fly brain and retina[18]. Another example is Fibronectin-domain III containing 5 (FNDC5), a glycosylated type 1 membrane protein that is highly enriched in skeletal muscle. FNDC5 can be proteolytically cleaved into an N-terminal fragment known as irisin, which is then released into circulation[88]. Recent studies have demonstrated that peripheral delivery of irisin reduces neuroinflammation and rescues cognitive decline in two separate mouse models of AD, and is a central modulator of cognitive function[32]. Likewise, the lysosomal protease CTSB is secreted from skeletal muscle into circulation in response to exercise and is required for the full manifestation of exercise-associated benefits on the CNS, including increases in the levels of hippocampal BDNF and re-activation of neurogenesis[33]. This suggests that maintenance of the skeletal muscle secretome may be central to the regulation of CNS aging and disease.

Here, and for the first time in mammals, we provide direct evidence demonstrating the CNS benefits of maintaining skeletal muscle proteostasis throughout aging. We find that life-long mild overexpression of TFEB in skeletal muscle in cTFEB;HSACre transgenic mice reduces the development of age-associated biochemical hallmarks in the hippocampus, ultimately preserving cognitive function in the aging brain. Importantly, we document that these benefits occur without any detectable expression of our transgene in the CNS, suggesting that the observed reductions in proteotoxicity and neuroinflmmation, as well as the improved neurocognitive performance of aged cTFEB;HSACre mice are due to the overexpression of TFEB solely in the skeletal muscle.

We also report significant transcriptional remodeling of the hippocampus in response to enhanced skeletal muscle proteostasis. In-depth transcriptional studies of the aging mouse brain point to key metabolic pathways, including the dysregulation of ion homeostasis, disruption of neurotransmission and ribosome biogenesis as key biological process exhibiting differential regulation with aging[2,90]. In particular, multiple studies have shown that down-regulated genes during aging are enriched with genes related to synaptic transmission and plasticity (reviewed here[3]). It is particularly interesting that manipulation of skeletal muscle proteostasis modulates expression of similar key functional enrichment categories in the aging hippocampus in a sex-dependent manner. While it is unclear whether these differential responses between male and female hippocampi to the enhancement of skeletal muscle proteostasis reflect local differences in the CNS or peripheral differences in the expression, secretion or trafficking of circulating signals, they underscore the fundamental need to examine sex differences contributing to the biology of aging.

Tauopathies are clinically, biochemically and morphologically heterogeneous neurodegenerative diseases characterized by the deposition of abnormal aggregates of tau in the brain. The MAPT P301S model recapitulates multiple aspects of tauopathies, including microglial activation, filamentous tau inclusions and synapse loss[67]. Our studies indicate that enhancing skeletal muscle proteostasis has significant benefits on multiple markers of gliosis, reducing the number of astrocytes and the volume of microglia present in the hippocampus. Glial cell size and morphology have been directly linked to their inflammatory status, suggesting that enhancing muscle proteostasis in MAPT P301S transgenic mice reduces microglial and astrocyte activation, ultimately reducing neuroinflammation. Indeed, we also detected significantly reduced transcriptional activation of the nCounter AD microglial activation panel. This highlights both the robust pro-inflammatory state associated with tau pathogenesis, as well as the intriguing possibility that manipulation of skeletal muscle proteostasis pathways may represent a novel target for modulation of neuroinflammation in the context of neurodegenerative disease.

Peripheral circulating factors have recently arisen as novel regulators of CNS metabolism and function [18,29,32,33,39]. Although the precise mechanisms underlying the neurotrophic and neuroprotective effects of these factors remain poorly understood, most of them have been reported to work through inhibition of neuroinflammation[23,27,28,32], consistent with our findings in aging and MAPT P301S models. Through our proteomics analysis, we identified multiple differentially expressed proteins in TFEB-overexpressing skeletal muscle that are predicted to be secreted through classical and non-classical mechanisms. Interestingly, our highest

493 expressed factor was CTSB, and we confirmed higher levels of circulating CTSB in the serum of
494 cTFEB;HSACre transgenic mice. CTSB has been proposed to cross the blood-brain barrier [33].
495 Furthermore, administration of recombinant CTSB to adult hippocampal progenitor cells in vitro
496 increases levels of BDNF [33]. In vivo, extracellular CTSB remodels the extracellular matrix [91] ,
497 enhancing axonal outgrowth through degradation of chondroitin sulfate[92,93]. Furthermore, high
498 CTSB expression levels in the hippocampus has been reported in low-anxiety mouse lines[94,95],
499 suggesting that CTSB may play important roles in maintaining neuronal homeostasis in brain
500 regions with high relevance for both aging and age-associated neurodegenerative disease. Our
501 results imply that additional research into the role and function of circulating proteoases and
502 their ability to remodel the CNS may be warranted.

503 Over the last ten years, there has been growing evidence that suggests prominent contributions
504 of the periphery to the etiology of neurodegenerative diseases. Our discovery that skeletal
505 muscle proteostasis can be a crucial site for regulation of CNS health and function provides
506 compelling evidence for a new therapeutic delivery avenue into the brain, providing a currently
507 unexplored new diagnostic and therapeutic intervention site (i.e. Skeletal muscle) for
508 lengthening cognitive healthspan.

509

METHODS

Generation of fxSTOP-TFEB transgenic mice.

We used a pCMV-human TFEB expressing vector from Origene (clone # sc122773), used previously [40]. We cloned a 3x-FLAG fragment via insertion into the Acc65I and Pac1 restriction sites of the targeting vector. The fxSTOP-TFEB vector was generated in multiple steps, as follows: (1) 5′ and 3′ targeting arms were inserted by PCR onto the ends of a minimal 1.8 kb, chloramphenicol-resistant vector; (2) an ampicillin resistance cassette was cloned into the MluI, XmaI sites of the targeting vector; (3) an 1.1 kb fragment encoding the actin promoter, a loxP site, a 3x-FLAG tag fused to EGFP was cloned into the NheI, PacI restriction sites of the targeting vector; (4) a 2.8 kb fragment containing the second loxP site, followed by 3x-FLAG-human TFEB sequence. The final fxSTOP-FLAG-human TFEB vector was microinjected into C57BL/6J:C3H/HeJ F1 hybrid oocytes. Of six founders identified, two gave rise to fxSTOP-FLAG-human TFEB lines with comparable phenotypes. Of these lines, we chose to focus our studies principally on line 419. The presence of the floxed 3x-FLAG-eGFP STOP-3x-FLAG-human TFEB cassette is verified by allele dependent qPCR genotyping analysis with each generation (Transnetyx), and expression of the 3x-FLAG-eGFP sequence (upstream of the STOP codon) in single transgenic fxSTOP-TFEB mice is assessed every other generation. We confirmed excision of 3x-FLAG-EGFP-STOP cassette in the presence of Cre-recombinase by crossing fxSTOP-TFEB transgenic female mice with HSA-Cre transgenic mice, (JAX Strain No: 006139 | HSA-Cre79), and corresponds to the HSA-Cre driver mouse line from the laboratory of Dr. Judith Melki. TdTomato mice (B6.Cg-Gt(ROSA)26Sor$^{tm9(CAG-tdTomato)Hze/J}$, JAX Strain #:007909) express robust tdTomato fluorescence following Cre-mediated recombination, is congenic on the C57BL/6J genetic background and were also obtained from JAX. The MAPT P301S line (Stock No: 008169) originated in the laboratory of Dr. Virginia Lee. cTFEB;HSACre;MAPT P301S transgenic mice were generated by crossing fxSTOP-TFEB females to MAPT P301S males. Female double transgenic offspring was then crossed with homozygote HSA-Cre transgenic males. All commercially available lines were obtained directly from JAX. All lines have been maintained in a C57/B6 background for over ten generations in our lab. Age-matched littermates were used for all experiments. Mice were housed in a temperature- and humidity-controlled environment on a 12-hour light/dark cycle with food and water ad libitum. Mice of both sexes were used for all experiments in equal numbers, or as close to equal numbers as possible. All animal experimentation adhered to NIH guidelines and was approved by and performed in accordance with the University of California, San Diego,

Duke University and University of Alabama at Birmingham Institutional Animal Care and Use. The fxSTOp-TFEB line of transgenic mice is available for sharing with academic institutions free-of-charge. For-profit institutions will adhere to UCSD's policy regarding copyrighted material.

Tissue Collections

Animals were anesthetized with 3.8% Avertin Solution. All animals received a transcardial perfusion with 60 mLs of cold 1x PBS. Half of the tissue (right/left muscle, right/left hemi-brain) was post-fixed in 4% PFA for less than 24 hours before being transferred to 30% sucrose for another 24 hrs, the other half was flash-frozen in liquid nitrogen for RNA and protein analyses.

RT-PCR Analysis

Flash frozen perfused isolated mouse tissues (Quadricep, Hippocampus) were placed in plastic tubes with silica beads (MP Biomedical, 116913100) and homogenized in TRIzol (Invitrogen, 15596026). RNA was extracted via standard phenol-chloroform procedures followed by DNase digestion (Thermo Fisher, AM2238). cDNA was generated using iScript (Bio-Rad Technologies, 1708891). Quantitative PCR was run using Sybrgreen (Life Technologies, 4309155) for chemical detection (Applied Biosystems; QuantStudio 3). Enrichment was determined based on double-delta CT value. Primers were ordered from IDT Predesigned qPCR Assays unless otherwise specified. Primers used are listed in Primer Table 1.

ImmunoBlot Analysis

Protein lysates from muscle tissue was prepared as previously described [40,42]. Protein concentration was quantified using a Pierce™ BCA Protein Assay (23227). Fifty µg of homogenized proteins were loaded per lane, and after running Any KD, 10%, or 4-15% Mini-PROTEAN TGX Gels (BioRad, 4568124, 4561034, and 4561084), samples were transferred to 0.2 µm (for LC3) or 0.45 µm (for everything else) PVDF membranes (BioRad, 162-0175 and 1704275), which were blocked in 5% BSA in PBS at RT for 1 hr. Membranes were incubated with anti-FLAG antibody (Sigma, M2, 1:1000), anti-Lamp1 antibody (Novus Bio, NB600-956, 1:1000), anti-LC3 antibody (Cell Signaling, 2775S, 1:1000), anti-p62 (MBC, PM045, 1:1000), anti-cathepsin B (Cell Signaling, 31718S, 1:1000) or anti-GAPDH (Invitrogen, AM4300, 1:5000) in PBS-T with 5% BSA at 4°C overnight. The primary antibody was visualized with horseradish-peroxidase conjugated anti-rabbit at 1:5,000 (Cell Signaling, 7074P2) and enhanced

chemiluminescence (BioRad, 170-5060) or goat-anti-mouse IgG 680 (Invitrogen, A21058) at 1:10,000. Densitometry analysis was performed using the BioRad Image Lab 6.1 software application.

Cathespin B ELISA Analysis

Fifty µl of serum (collected via blood cardiac puncture and isolated via standard coagulation/centrifugation protocols) was diluted 1:1 by reconstituting with sample dilutant buffer (Abcam, ab119585). Diluted samples were processed following kit instructions, and imaged at 450 nm (Tecan, Infinite M plex). Amount of cathepsin B was determined using a standard dilution curve of known concentration.

Histological Studies

Tissue was embedded in OCT (TissueTek, 4583), frozen utilizing 2-methylbutane (VWR, 103525-278) submerged in liquid nitrogen and stored at -80C until used. All samples were sectioned on a standing cryostat (Leica). Sections of brain were 20 microns, while muscle tissue was 15 microns thick. For immunohistochemistry, sections were permeabilized with .25% Triton for 15 mins and blocked with 4% BSA for 30 minutes-1 hour. Brain sections were then incubated with anti-GFAP (ab4674, Abcam, 1:200), anti-Iba1 (Wako, 019-19741, 1:200), and anti-AT8 TAU (Invitrogen, MN1020, 1:100) while muscle sections were incubated with anti-laminin (Sigma, L9393, 1:200), anti-FLAG (Sigma, F1804, 1:1000), anti-LC3 (Cell Signaling, 2775S, 1:200), anti-ubiquitin (Abcam, ab7780 1:100) and anti-P62 (MBL, PM045, 1:200) overnight at 4°C and incubated with secondary antibodies at RT for 1 hour (both diluted in 4% BSA). Next the slides were washed with Hoescht (Thermo Scientific, 62249, 1:5000) and mounted with prolong glass (Invitrogen, P36984).All slides were washed with 1X PBS three times for 5 minutes each between steps.

Slides were imaged in the UAB HIRF HRIF Confocal/Light Microscopy Core utilizing the 10x objective on the Nikon A15R/SIM Confocal microscope. Z-stacks of the entire hippocampus area/section were collected, and max intensity projections were generated using FIJI. Lipofuscin imaging was performed using an epifluorescent Nikon light microscope with a 20x objective. For TdTomato imaging, stitched whole-section z-stacks were acquired using a Nikon A1R HD25 confocal microscope of nuclei in the blue channel and native TdTomato fluorescence in the red channel.

For quantification of astrocyte and/or microglia parameters, raw ND2 files were uploaded to the NIS elements platform and thresholds were set to eliminate background in each channel in order to delineate each object. Morphometric information was collected in addition to the automated counting of objects. A size exclusion parameter was used for GFAP positive objects under 10 microns, IBA-1 positive objects under 15 microns, and any object larger than 5,000 microns were all excluded due to standard assessments of cell sizes.

Quantitative proteomics sample preparation and data-independent acquisition mass spectrometry.

We identified distinct protein species from crude total extractions of whole quadriceps muscle by mass spectrometry after trypsin digestion, in collaboration with the University of Washington Nathan Shock Center Protein Phenotypes of Aging Proteomics Core. Quadriceps muscle powder samples were processed and digested using S-Trap Micro Spin Column (Protifi, C02-micro-80) following the manufacturer's protocol. SDS (5%) lysis and solubilization buffer were added to liver powder samples and homogenized on ice using a sonicator probe. Protein concentrations were determined using Pierce BCA Protein Assay Kit (Thermo Fisher Scientific, PI23227). Proteins were digested at 1 ug trypsin to 25 ug protein ratio on S-Trap at 47°C for 1 h. Peptides extracted from S-Trap were dried with a vacuum concentrator and reconstituted in 0.1% formic acid in water prior to mass spectrometry acquisition. Data were acquired using data-independent acquisition (DIA) on a Thermo EASY-nLC 1000 and a Thermo Q-Exactive HF orbitrap mass spectrometer. Peptides were separated using PicoFrit Self-Packed Columns (360 µm OD x 75 µm ID; New Objective, Woburn, MA) packed to 30 cm with 3 µm ReproSil-Pur C18 beads (ESI Source Solutions, r13.aq.0001). The trap column was packed to 2 cm with same C18 beads using 360 µm OD x 150 µm ID fused silica capillary fritted with Kasil on one end. Solvent A was 0.1% formic acid in water, and solvent B was 0.1% formic acid in 80% acetonitrile. For each injection, 1 µg of sample was loaded and eluted using a 90-min gradient from 5% to 45% B at 250 nL/min. DIA methods followed the chromatogram library workflow as described in detail previously [96]. All muscle samples were pooled in equal ratio to create a muscle library sample. The library samples were used to generate chromatogram libraries using the strategy described before [97]. Thermo Q Exactive HF MS was used to acquire six gas phase fractionated runs spanning a total mass range of 400 to 1000 m/z, each with staggered 4 m/z narrow precursor isolation windows [98]. EncyclopeDIA software suite was used to generate a chromatogram library [96] and retention time models for all peptides detected at 1% FDR determined by Percolator [99]. For quantitative DIA run, equal amounts of protein were used for

each sample. A 24 × 24 m/z staggered window from 400.43190 to 1000.7048 m/z was used as described previously [98]. EncyclopeDIA software suite was used to search the chromatogram library with calibrated retention time and quantify peptides and proteins in each sample.

Proteomics Analysis

A linear model was fit to the protein level data using the Bioconductor limma package [100], and the estimated SVs were adjusted as covariates in our model. The limma package uses empirical Bayes moderated statistics, which improves power by 'borrowing strength' between proteins in order to moderate the residual variance [101]. Adjusted P value was calculated with Benjamini-Hochberg method across groups (young transgenic, young control, old transgenic, and old control). Proteins were sorted for significant differential expression with dplyr using a cutoff of less than 5% FDR and greater than $|\pm 0.58496|$ $\log_2$ foldchange in young and old cohorts as a change due to skeletal muscle overexpression of humanized TFEB. Volcano plots were created with ggplot and ggrepel. Significantly upregulated proteins in cTFEB;HSA-Cre mice were queried using the KEGG pathway analyzer, which is a feature of STRING's web tool [54]. Bar graphs were created in Rstudio with the ggplot2 and forcats packages.

Significantly upregulated proteins, up to two degrees from TFEB, were entered into STRINGdb for functional network analysis. A confidence interaction score of 0.70 and MCL clustering was applied to the networks. The networks were exported from STRING and imported into Cytoscape for further style editing [102]. Predicted secreted proteins were identified by comparing the significantly differentially expressed proteins to the mus musculus secretome from VerSeDa[61].

Gene Expression Analysis.

RNA Sequencing

RNA was extracted as mentioned above from flash frozen hippocampal tissue or tissue was extracted by Novogene (Novogene Corporation INC, Sacramento, CA, United States) for four biological replicates (sex/genotype) and checked for quality. mRNA libraries were prepared by Novogene and bulk RNA-seq analysis was performed via NovaSeq PE150 (Illumina, San Diego, CA, United States) high throughput sequencing.

Nanostring nCounter AD panel

Assays were performed with 100 ng aliquots of RNA using the NanoString nCounter Analysis system (NanoString Technologies, Seattle, WA, USA) at the UAB Nanostring Core, following previously described and established protocols [73]. Counts for target genes were normalized to house-keeping genes included in the panel (*Cltc, Gapdh, Gusb, Hprt, Pgk1, Tubb5*). After codeset hybridization overnight, the samples were washed and immobilized to a cartridge using the NanoString nCounter Prep Station. Cartridges were scanned in the nCounter Digital Analyzer at 555 fields of view for the maximum level of sensitivity. Gene expression was normalized using NanoStringNorm R package. Specifically, background correction was performed using the negative control at the cutoff of mean + 2 standard deviation. All p values were adjusted using a false discovery rate (FDR) correction of 1% for multiple comparisons. Housekeeping genes were used to for normalization based on geometric mean. Data and heat analyses were performed in the nSolver Analysis Software 2.0. Gene expression values were presented as the percentage of the MAPT P301S group for comparison of MAPT P301S pathogenesis to the cTFEB;HSACre;MAPT P301S cohort.

Mouse Phenotyping and Behavioral Studies.

Barnes Maze

The Barnes maze apparatus is an opaque Plexiglas disc 75 cm in diameter elevated 58 cm above the floor by a tripod. Twenty holes, 5 cm in diameter, are located 5 cm from the perimeter, and a black Plexiglas escape box (19 x 8 x 7 cm) is placed under one of the holes. Distinct spatial cues are located all around the maze and are kept constant throughout the study. On the first day of testing, a training session was performed, which consists of placing the mouse in the escape box for one minute. After the one minute habituation period, the first session was started. At the beginning of each session, the mouse was placed in the middle of the maze in a 10 cm high cylindrical black start chamber. After 10 seconds the start chamber was removed, a buzzer (80 dB) and a light (400 lux) were turned on, and the mouse was set free to explore the maze. The session ended when the mouse entered the escape tunnel or after 3 min elapsed. When the mouse entered the escape tunnel, the buzzer was turned off and the mouse was allowed to remain in the dark for one minute. When the mouse did not enter the tunnel by itself it was gently put in the escape box for one minute. The tunnel was always located underneath the same hole (stable within the spatial environment), which was randomly determined for each mouse. Mice were tested once a day for 4 days for the acquisition portion of the study. For the 5th test (probe test), the escape tunnel was removed and the mouse was

allowed to freely explore the maze for 3 min. The time spent in each quadrant was determined and the percent time spent in the target quadrant (the one originally containing the escape box) was compared with the average percent time in the other three quadrants. This was a direct test of spatial memory as there was no potential for local cues to be used in the mouse's behavioral decision. Two weeks later the mice were tested again with the escape box in the original position (retention test). This allows for the examination of long term memory. Finally, on the day after this test, the escape tunnel was moved to a new location (90 degrees from the original position) and the behavior of the mouse was recorded. This is called the reversal test and it allows for the examination of perseveration at the old hole as well as the working memory strategies the mice adopted to locate the new tunnel location. Each session was videotaped and scored by an experimenter blind to the genotype of the mouse. Measures recorded include the latency to enter the escape box and the number of errors made per session. Errors are defined as nose pokes and head deflections over any hole that did not have the tunnel beneath it. The probe data were analyzed using Noldus Ethovision software to determine time spent in each quadrant of the maze as well as to assess activity measures.

Novel Object Recognition

Mice were individually habituated to a 51cm x 51cm x 39cm open field for 5 min. Mice were then tested with two identical objects placed in the field (either two 250 ml amber bottles or two clear plastic cylinders 6x6x16cm half filled with glass marbles). An individual animal was allowed to explore for 5 min, now with the objects present. After two such trials (each separated by 1 minute in a holding cage), the mouse was tested in the object novelty recognition test in which a novel object replaced one of the familiar objects (for example, an amber bottle if the cylinders were initially used). All objects and the arena were thoroughly cleaned with 70% ethanol between trials to remove odors. Behavior was video recorded and then scored for number contacts (touching with nose or nose pointing at object and within 0.5 cm of object) and/or for time contacting the objects. Habituation to the objects across the familiarization trials (decreased contacts) was an initial measure of learning and then renewed interest (increased contacts) in the new object indicated successful object memory. Recognition indexes were calculated using the following formula: # contacts during test/(# contacts in last familiarization trial + # contacts during test). Values greater than 0.5 indicate increased interest, whereas values less than 0.5 indicate decreased interest in the object during the test relative to the final familiarization trial.

729 **Statistical Analysis**

730 All data were analyzed by t-test, 1-way, 2-way or 3-way between-subject ANOVA with post hoc
731 comparisons depending on the number of variables and groups in each analysis. For ANOVA, if
732 statistical significance ($p < 0.05$) was achieved, we performed post hoc analysis to account for
733 multiple comparisons. The level of significance (α) was always set at 0.05. Survival curves were
734 analyzed using Log-rank (Mantel-Cox) Test. Data were analyzed using Prism 7 (GraphPad
735 Software, La Jolla, CA) and are represented as means and standard error of the means. All
736 experiments and data analyses were conducted in a blinded fashion. All data were prepared for
737 analysis with standard spread sheet software (Microsoft Excel).

738

739

740

741

742

743

744

745

746

747

748

749

750

751

REFERENCES

1 Lopez-Otin, C., Blasco, M. A., Partridge, L., Serrano, M. & Kroemer, G. The hallmarks of aging. *Cell* **153**, 1194-1217, doi:10.1016/j.cell.2013.05.039 (2013).

2 Mattson, M. P. & Arumugam, T. V. Hallmarks of Brain Aging: Adaptive and Pathological Modification by Metabolic States. *Cell metabolism* **27**, 1176-1199, doi:10.1016/j.cmet.2018.05.011 (2018).

3 Ham, S. & Lee, S. V. Advances in transcriptome analysis of human brain aging. *Exp Mol Med* **52**, 1787-1797, doi:10.1038/s12276-020-00522-6 (2020).

4 Aman, Y. *et al.* Autophagy in healthy aging and disease. *Nat Aging* **1**, 634-650, doi:10.1038/s43587-021-00098-4 (2021).

5 Hara, T. *et al.* Suppression of basal autophagy in neural cells causes neurodegenerative disease in mice. *Nature* **441**, 885-889, doi:10.1038/nature04724 (2006).

6 Komatsu, M. *et al.* Loss of autophagy in the central nervous system causes neurodegeneration in mice. *Nature* **441**, 880-884, doi:10.1038/nature04723 (2006).

7 Mansueto, G. *et al.* Transcription Factor EB Controls Metabolic Flexibility during Exercise. *Cell metabolism* **25**, 182-196, doi:10.1016/j.cmet.2016.11.003 (2017).

8 Kim, K. H. *et al.* Autophagy deficiency leads to protection from obesity and insulin resistance by inducing Fgf21 as a mitokine. *Nat Med* **19**, 83-92, doi:10.1038/nm.3014 (2013).

9 Kustermann, M. *et al.* Loss of the novel Vcp (valosin containing protein) interactor Washc4 interferes with autophagy-mediated proteostasis in striated muscle and leads to myopathy in vivo. *Autophagy* **14**, 1911-1927, doi:10.1080/15548627.2018.1491491 (2018).

10 Lapierre, L. R. *et al.* The TFEB orthologue HLH-30 regulates autophagy and modulates longevity in Caenorhabditis elegans. *Nat Commun* **4**, 2267, doi:10.1038/ncomms3267 (2013).

11 Pyo, J. O. *et al.* Overexpression of Atg5 in mice activates autophagy and extends lifespan. *Nat Commun* **4**, 2300, doi:10.1038/ncomms3300 (2013).

12 Simonsen, A. *et al.* Promoting basal levels of autophagy in the nervous system enhances longevity and oxidant resistance in adult Drosophila. *Autophagy* **4**, 176-184, doi:5269 [pii] (2008).

13 Colman, R. J. *et al.* Caloric restriction delays disease onset and mortality in rhesus monkeys. *Science* **325**, 201-204, doi:10.1126/science.1173635 (2009).

14 Eisenberg, T. *et al.* Induction of autophagy by spermidine promotes longevity. *Nature cell biology* **11**, 1305-1314, doi:10.1038/ncb1975 (2009).

15 Harrison, D. E. *et al.* Rapamycin fed late in life extends lifespan in genetically heterogeneous mice. *Nature* **460**, 392-395, doi:10.1038/nature08221 (2009).

16 Settembre, C. *et al.* TFEB controls cellular lipid metabolism through a starvation-induced autoregulatory loop. *Nature cell biology* **15**, 647-658, doi:10.1038/ncb2718 (2013).

17 Demontis, F., Patel, V. K., Swindell, W. R. & Perrimon, N. Intertissue control of the nucleolus via a myokine-dependent longevity pathway. *Cell Rep* **7**, 1481-1494, doi:10.1016/j.celrep.2014.05.001 (2014).

18 Rai, M. *et al.* Proteasome stress in skeletal muscle mounts a long-range protective response that delays retinal and brain aging. *Cell metabolism* **33**, 1137-1154 e1139, doi:10.1016/j.cmet.2021.03.005 (2021).

19 Durieux, J., Wolff, S. & Dillin, A. The cell-non-autonomous nature of electron transport chain-mediated longevity. *Cell* **144**, 79-91, doi:10.1016/j.cell.2010.12.016 (2011).

20 Taylor, R. C. & Dillin, A. XBP-1 is a cell-nonautonomous regulator of stress resistance and longevity. *Cell* **153**, 1435-1447, doi:10.1016/j.cell.2013.05.042 (2013).

21 Demontis, F. & Perrimon, N. FOXO/4E-BP signaling in Drosophila muscles regulates organism-wide proteostasis during aging. *Cell* **143**, 813-825, doi:10.1016/j.cell.2010.10.007 (2010).

22 van Oosten-Hawle, P., Porter, R. S. & Morimoto, R. I. Regulation of organismal proteostasis by transcellular chaperone signaling. *Cell* **153**, 1366-1378, doi:10.1016/j.cell.2013.05.015 (2013).

23 Villeda, S. A. *et al.* The ageing systemic milieu negatively regulates neurogenesis and cognitive function. *Nature* **477**, 90-94, doi:10.1038/nature10357 (2011).

24 Conboy, I. M. *et al.* Rejuvenation of aged progenitor cells by exposure to a young systemic environment. *Nature* **433**, 760-764, doi:10.1038/nature03260 (2005).

25 Castellano, J. M. *et al.* Human umbilical cord plasma proteins revitalize hippocampal function in aged mice. *Nature* **544**, 488-492, doi:10.1038/nature22067 (2017).

26 Schaum, N. *et al.* Ageing hallmarks exhibit organ-specific temporal signatures. *Nature* **583**, 596-602, doi:10.1038/s41586-020-2499-y (2020).

27 Villeda, S. A. *et al.* Young blood reverses age-related impairments in cognitive function and synaptic plasticity in mice. *Nat Med* **20**, 659-663, doi:10.1038/nm.3569 (2014).

28 De Miguel, Z. *et al.* Exercise plasma boosts memory and dampens brain inflammation via clusterin. *Nature*, doi:10.1038/s41586-021-04183-x (2021).

29 Horowitz, A. M. *et al.* Blood factors transfer beneficial effects of exercise on neurogenesis and cognition to the aged brain. *Science* **369**, 167-173, doi:10.1126/science.aaw2622 (2020).

30 Ozek, C., Krolewski, R. C., Buchanan, S. M. & Rubin, L. L. Growth Differentiation Factor 11 treatment leads to neuronal and vascular improvements in the hippocampus of aged mice. *Sci Rep* **8**, 17293, doi:10.1038/s41598-018-35716-6 (2018).

31 Wrann, C. D. *et al.* Exercise induces hippocampal BDNF through a PGC-1α/FNDC5 pathway. *Cell metabolism* **18**, 649-659, doi:10.1016/j.cmet.2013.09.008 (2013).

32 Islam, M. R. *et al.* Exercise hormone irisin is a critical regulator of cognitive function. *Nat Metab* **3**, 1058-1070, doi:10.1038/s42255-021-00438-z (2021).

33 Moon, H. Y. *et al.* Running-Induced Systemic Cathepsin B Secretion Is Associated with Memory Function. *Cell metabolism* **24**, 332-340, doi:10.1016/j.cmet.2016.05.025 (2016).

34 White, P. J. *et al.* Protectin DX alleviates insulin resistance by activating a myokine-liver glucoregulatory axis. *Nat Med* **20**, 664-669, doi:10.1038/nm.3549 (2014).

35 Quinn, L. S., Anderson, B. G., Strait-Bodey, L., Stroud, A. M. & Argilés, J. M. Oversecretion of interleukin-15 from skeletal muscle reduces adiposity. *American Journal of Physiology-Endocrinology and Metabolism* **296**, E191-E202 (2009).

36 Boyle, P. A., Buchman, A. S., Wilson, R. S., Leurgans, S. E. & Bennett, D. A. Association of muscle strength with the risk of Alzheimer disease and the rate of cognitive decline in community-dwelling older persons. *Arch Neurol* **66**, 1339-1344, doi:10.1001/archneurol.2009.240 (2009).

37 Kim, J. *et al.* Association of muscle and visceral adipose tissues with the probability of Alzheimer's disease in healthy subjects. *Sci Rep* **9**, 949, doi:10.1038/s41598-018-37244-9 (2019).

38 Lourenco, M. V. *et al.* Exercise-linked FNDC5/irisin rescues synaptic plasticity and memory defects in Alzheimer's models. *Nat Med* **25**, 165-175, doi:10.1038/s41591-018-0275-4 (2019).

39 Gupta, R., Khan, R. & Cortes, C. J. Forgot to Exercise? Exercise Derived Circulating Myokines in Alzheimer's Disease: A Perspective. *Front Neurol* **12**, 649452, doi:10.3389/fneur.2021.649452 (2021).

40 Cortes, C. J. *et al.* Polyglutamine-expanded androgen receptor interferes with TFEB to elicit autophagy defects in SBMA. *Nat Neurosci* **17**, 1180-1189, doi:10.1038/nn.3787 (2014).

41 Cortes, C. J. & La Spada, A. R. Motor neuron degeneration in spinal and Bulbar Muscular Atrophy is a skeletal muscle-driven process: Relevance to therapy development and implications for related motor neuron diseases. *Rare Dis* **2**, e962402, doi:10.4161/2167549X.2014.962402 (2014).

42 Cortes, C. J. *et al.* Muscle expression of mutant androgen receptor accounts for systemic and motor neuron disease phenotypes in spinal and bulbar muscular atrophy. *Neuron* **82**, 295-307, doi:10.1016/j.neuron.2014.03.001 (2014).

43 Settembre, C. *et al.* TFEB links autophagy to lysosomal biogenesis. *Science* **332**, 1429-1433, doi:10.1126/science.1204592 (2011).

44 Palmieri, M. *et al.* Characterization of the CLEAR network reveals an integrated control of cellular clearance pathways. *Human molecular genetics* **20**, 3852-3866, doi:10.1093/hmg/ddr306 (2011).

45 Sardiello, M. *et al.* A gene network regulating lysosomal biogenesis and function. *Science* **325**, 473-477, doi:10.1126/science.1174447 (2009).

46 Morgan, T. E. *et al.* The mosaic of brain glial hyperactivity during normal ageing and its attenuation by food restriction. *Neuroscience* **89**, 687-699, doi:10.1016/s0306-4522(98)00334-0 (1999).

47 van Praag, H., Shubert, T., Zhao, C. & Gage, F. H. Exercise enhances learning and hippocampal neurogenesis in aged mice. *The Journal of neuroscience : the official journal of the Society for Neuroscience* **25**, 8680-8685, doi:10.1523/jneurosci.1731-05.2005 (2005).

48 Zhu, H., Guo, Q. & Mattson, M. P. Dietary restriction protects hippocampal neurons against the death-promoting action of a presenilin-1 mutation. *Brain Res* **842**, 224-229, doi:10.1016/s0006-8993(99)01827-2 (1999).

49 Duan, W. & Mattson, M. P. Dietary restriction and 2-deoxyglucose administration improve behavioral outcome and reduce degeneration of dopaminergic neurons in models of Parkinson's disease. *J Neurosci Res* **57**, 195-206, doi:10.1002/(SICI)1097-4547(19990715)57:2<195::AID-JNR5>3.0.CO;2-P (1999).

50 Choi, S. H. *et al.* Combined adult neurogenesis and BDNF mimic exercise effects on cognition in an Alzheimer's mouse model. *Science* **361**, doi:10.1126/science.aan8821 (2018).

51 Leu, M. *et al.* Erbb2 regulates neuromuscular synapse formation and is essential for muscle spindle development. *Development* **130**, 2291-2301 (2003).

52 Madisen, L. *et al.* A robust and high-throughput Cre reporting and characterization system for the whole mouse brain. *Nat Neurosci* **13**, 133-140, doi:10.1038/nn.2467 (2010).

53 Giacomello, E. *et al.* Age Dependent Modification of the Metabolic Profile of the Tibialis Anterior Muscle Fibers in C57BL/6J Mice. *Int J Mol Sci* **21**, doi:10.3390/ijms21113923 (2020).

54 Szklarczyk, D. *et al.* The STRING database in 2021: customizable protein-protein networks, and functional characterization of user-uploaded gene/measurement sets. *Nucleic Acids Res* **49**, D605-D612, doi:10.1093/nar/gkaa1074 (2021).

55 Decressac, M. *et al.* TFEB-mediated autophagy rescues midbrain dopamine neurons from alpha-synuclein toxicity. *Proceedings of the National Academy of Sciences of the United States of America* **110**, E1817-1826, doi:10.1073/pnas.1305623110 (2013).

56 Spampanato, C. *et al.* Transcription factor EB (TFEB) is a new therapeutic target for Pompe disease. *EMBO Mol Med* **5**, 691-706, doi:10.1002/emmm.201202176 (2013).

57 Klionsky, D. J. *et al.* Guidelines for the use and interpretation of assays for monitoring autophagy (3rd edition). *Autophagy* **12**, 1-222, doi:10.1080/15548627.2015.1100356 (2016).

58 Jiao, J. & Demontis, F. Skeletal muscle autophagy and its role in sarcopenia and organismal aging. *Curr Opin Pharmacol* **34**, 1-6, doi:10.1016/j.coph.2017.03.009 (2017).

59 Mancinelli, R. *et al.* Biological Aspects of Selected Myokines in Skeletal Muscle: Focus on Aging. *Int J Mol Sci* **22**, doi:10.3390/ijms22168520 (2021).

60 Rai, M. & Demontis, F. Systemic Nutrient and Stress Signaling via Myokines and Myometabolites. *Annu Rev Physiol* **78**, 85-107, doi:10.1146/annurev-physiol-021115-105305 (2016).

61 Cortazar, A. R., Oguiza, J. A., Aransay, A. M. & Lavin, J. L. VerSeDa: vertebrate secretome database. *Database (Oxford)* **2017**, doi:10.1093/database/baw171 (2017).

62 Lehallier, B. *et al.* Undulating changes in human plasma proteome profiles across the lifespan. *Nature Medicine* **25**, 1843-1850, doi:10.1038/s41591-019-0673-2 (2019).

63 Joly-Amado, A. *et al.* CCL2 Overexpression in the Brain Promotes Glial Activation and Accelerates Tau Pathology in a Mouse Model of Tauopathy. *Front Immunol* **11**, 997, doi:10.3389/fimmu.2020.00997 (2020).

64 Frakes, A. E. *et al.* Microglia induce motor neuron death via the classical NF-kappaB pathway in amyotrophic lateral sclerosis. *Neuron* **81**, 1009-1023, doi:10.1016/j.neuron.2014.01.013 (2014).

65 Islam, O., Gong, X., Rose-John, S. & Heese, K. Interleukin-6 and neural stem cells: more than gliogenesis. *Mol Biol Cell* **20**, 188-199, doi:10.1091/mbc.E08-05-0463 (2009).

66 Leibinger, M. *et al.* Interleukin-6 contributes to CNS axon regeneration upon inflammatory stimulation. *Cell Death Dis* **4**, e609, doi:10.1038/cddis.2013.126 (2013).

67 Yoshiyama, Y. *et al.* Synapse loss and microglial activation precede tangles in a P301S tauopathy mouse model. *Neuron* **53**, 337-351, doi:10.1016/j.neuron.2007.01.010 (2007).

68 Moloney, C. M., Lowe, V. J. & Murray, M. E. Visualization of neurofibrillary tangle maturity in Alzheimer's disease: A clinicopathologic perspective for biomarker research. *Alzheimers Dement* **17**, 1554-1574, doi:10.1002/alz.12321 (2021).

69 Jurga, A. M., Paleczna, M. & Kuter, K. Z. Overview of General and Discriminating Markers of Differential Microglia Phenotypes. *Front Cell Neurosci* **14**, 198, doi:10.3389/fncel.2020.00198 (2020).

70 Rozovsky, I., Finch, C. E. & Morgan, T. E. Age-related activation of microglia and astrocytes: in vitro studies show persistent phenotypes of aging, increased proliferation, and resistance to down-regulation. *Neurobiol Aging* **19**, 97-103, doi:10.1016/s0197-4580(97)00169-3 (1998).

71 Godbout, J. P. *et al.* Exaggerated neuroinflammation and sickness behavior in aged mice following activation of the peripheral innate immune system. *FASEB J* **19**, 1329-1331, doi:10.1096/fj.05-3776fje (2005).

72 Sidoryk-Wegrzynowicz, M. *et al.* Astrocytes in mouse models of tauopathies acquire early deficits and lose neurosupportive functions. *Acta Neuropathol Commun* **5**, 89, doi:10.1186/s40478-017-0478-9 (2017).

73 Preuss, C. *et al.* A novel systems biology approach to evaluate mouse models of late-onset Alzheimer's disease. *Mol Neurodegener* **15**, 67, doi:10.1186/s13024-020-00412-5 (2020).

74 de Rojas, I. *et al.* Common variants in Alzheimer's disease and risk stratification by polygenic risk scores. *Nat Commun* **12**, 3417, doi:10.1038/s41467-021-22491-8 (2021).

75 Scelsi, M. A. *et al.* Genetic study of multimodal imaging Alzheimer's disease progression score implicates novel loci. *Brain* **141**, 2167-2180, doi:10.1093/brain/awy141 (2018).

76 Kim, B. H., Nho, K., Lee, J. M. & Alzheimer's Disease Neuroimaging, I. Genome-wide association study identifies susceptibility loci of brain atrophy to NFIA and ST18 in Alzheimer's disease. *Neurobiol Aging* **102**, 200 e201-200 e211, doi:10.1016/j.neurobiolaging.2021.01.021 (2021).

77 Li, G. *et al.* Association of GALC, ZNF184, IL1R2 and ELOVL7 With Parkinson's Disease in Southern Chinese. *Front Aging Neurosci* **10**, 402, doi:10.3389/fnagi.2018.00402 (2018).

78 Sherva, R. *et al.* Genome-wide association study of the rate of cognitive decline in Alzheimer's disease. *Alzheimers Dement* **10**, 45-52, doi:10.1016/j.jalz.2013.01.008 (2014).

79 Chai K, L. J., Zhang X, Gu H, Cao P, Ye W, Tang H, Liu J, Chen S, Wan F, Liu GL, Shen D. ARHGDIB Plays a Novel Role in the Braak Stages of Alzheimer's Diseases via the Immune Response Mediated by Microglia

Pre-print: Research Square, doi:10.21203/rs.3.rs-474315/v1 (2021).

80 Simon, M. J. *et al.* Transcriptional network analysis of human astrocytic endfoot genes reveals region-specific associations with dementia status and tau pathology. *Sci Rep* **8**, 12389, doi:10.1038/s41598-018-30779-x (2018).

81 Knopman, D. S. *et al.* Alzheimer disease. *Nat Rev Dis Primers* **7**, 33, doi:10.1038/s41572-021-00269-y (2021).

82 Wohlgemuth, S. E., Seo, A. Y., Marzetti, E., Lees, H. A. & Leeuwenburgh, C. Skeletal muscle autophagy and apoptosis during aging: effects of calorie restriction and life-long exercise. *Exp Gerontol* **45**, 138-148, doi:10.1016/j.exger.2009.11.002 (2010).

83 Grumati, P. *et al.* Autophagy is defective in collagen VI muscular dystrophies, and its reactivation rescues myofiber degeneration. *Nat Med* **16**, 1313-1320, doi:10.1038/nm.2247 (2010).

84 He, C., Sumpter, R., Jr. & Levine, B. Exercise induces autophagy in peripheral tissues and in the brain. *Autophagy* **8**, 1548-1551, doi:10.4161/auto.21327 (2012).

85 Masiero, E. *et al.* Autophagy is required to maintain muscle mass. *Cell metabolism* **10**, 507-515, doi:10.1016/j.cmet.2009.10.008 (2009).

86 Raben, N. *et al.* Suppression of autophagy in skeletal muscle uncovers the accumulation of ubiquitinated proteins and their potential role in muscle damage in Pompe disease. *Human molecular genetics* **17**, 3897-3908, doi:10.1093/hmg/ddn292 (2008).

87 Vainshtein, A., Grumati, P., Sandri, M. & Bonaldo, P. Skeletal muscle, autophagy, and physical activity: the menage a trois of metabolic regulation in health and disease. *J Mol Med (Berl)* **92**, 127-137, doi:10.1007/s00109-013-1096-z (2014).

88 Bostrom, P. *et al.* A PGC1-alpha-dependent myokine that drives brown-fat-like development of white fat and thermogenesis. *Nature* **481**, 463-468, doi:10.1038/nature10777 (2012).

89 Otaka, N. *et al.* Myonectin Is an Exercise-Induced Myokine That Protects the Heart From Ischemia-Reperfusion Injury. *Circ Res* **123**, 1326-1338, doi:10.1161/CIRCRESAHA.118.313777 (2018).

90 Ximerakis, M. *et al.* Single-cell transcriptomic profiling of the aging mouse brain. *Nat Neurosci* **22**, 1696-1708, doi:10.1038/s41593-019-0491-3 (2019).

91 Vizovisek, M., Fonovic, M. & Turk, B. Cysteine cathepsins in extracellular matrix remodeling: Extracellular matrix degradation and beyond. *Matrix Biol* **75-76**, 141-159, doi:10.1016/j.matbio.2018.01.024 (2019).

92 Tran, A. P., Sundar, S., Yu, M., Lang, B. T. & Silver, J. Modulation of Receptor Protein Tyrosine Phosphatase Sigma Increases Chondroitin Sulfate Proteoglycan Degradation through Cathepsin B Secretion to Enhance Axon Outgrowth. *The Journal of neuroscience : the official journal of the Society for Neuroscience* **38**, 5399-5414, doi:10.1523/JNEUROSCI.3214-17.2018 (2018).

93 Saini, M. G. & Bix, G. J. Oxygen-glucose deprivation (OGD) and interleukin-1 (IL-1) differentially modulate cathepsin B/L mediated generation of neuroprotective perlecan LG3 by neurons. *Brain Res* **1438**, 65-74, doi:10.1016/j.brainres.2011.12.027 (2012).

94 Muigg, P. *et al.* Differential stress-induced neuronal activation patterns in mouse lines selectively bred for high, normal or low anxiety. *PloS one* **4**, e5346, doi:10.1371/journal.pone.0005346 (2009).

95 Czibere, L. *et al.* Profiling trait anxiety: transcriptome analysis reveals cathepsin B (Ctsb) as a novel candidate gene for emotionality in mice. *PloS one* **6**, e23604, doi:10.1371/journal.pone.0023604 (2011).

96 Searle, B. C. *et al.* Chromatogram libraries improve peptide detection and quantification by data independent acquisition mass spectrometry. *Nat Commun* **9**, 5128, doi:10.1038/s41467-018-07454-w (2018).

97 Pino, L. K., Just, S. C., MacCoss, M. J. & Searle, B. C. Acquiring and Analyzing Data Independent Acquisition Proteomics Experiments without Spectrum Libraries. *Mol Cell Proteomics* **19**, 1088-1103, doi:10.1074/mcp.P119.001913 (2020).

98 Amodei, D. *et al.* Improving Precursor Selectivity in Data-Independent Acquisition Using Overlapping Windows. *J Am Soc Mass Spectrom* **30**, 669-684, doi:10.1007/s13361-018-2122-8 (2019).

99 Kall, L., Canterbury, J. D., Weston, J., Noble, W. S. & MacCoss, M. J. Semi-supervised learning for peptide identification from shotgun proteomics datasets. *Nat Methods* **4**, 923-925, doi:10.1038/nmeth1113 (2007).

100 Ritchie, M. E. *et al.* limma powers differential expression analyses for RNA-sequencing and microarray studies. *Nucleic Acids Res* **43**, e47, doi:10.1093/nar/gkv007 (2015).

101 Smyth, G. K. Linear models and empirical bayes methods for assessing differential expression in microarray experiments. *Stat Appl Genet Mol Biol* **3**, Article3, doi:10.2202/1544-6115.1027 (2004).

102 Shannon, P. *et al.* Cytoscape: a software environment for integrated models of biomolecular interaction networks. *Genome Res* **13**, 2498-2504, doi:10.1101/gr.1239303 (2003).

Figure 1

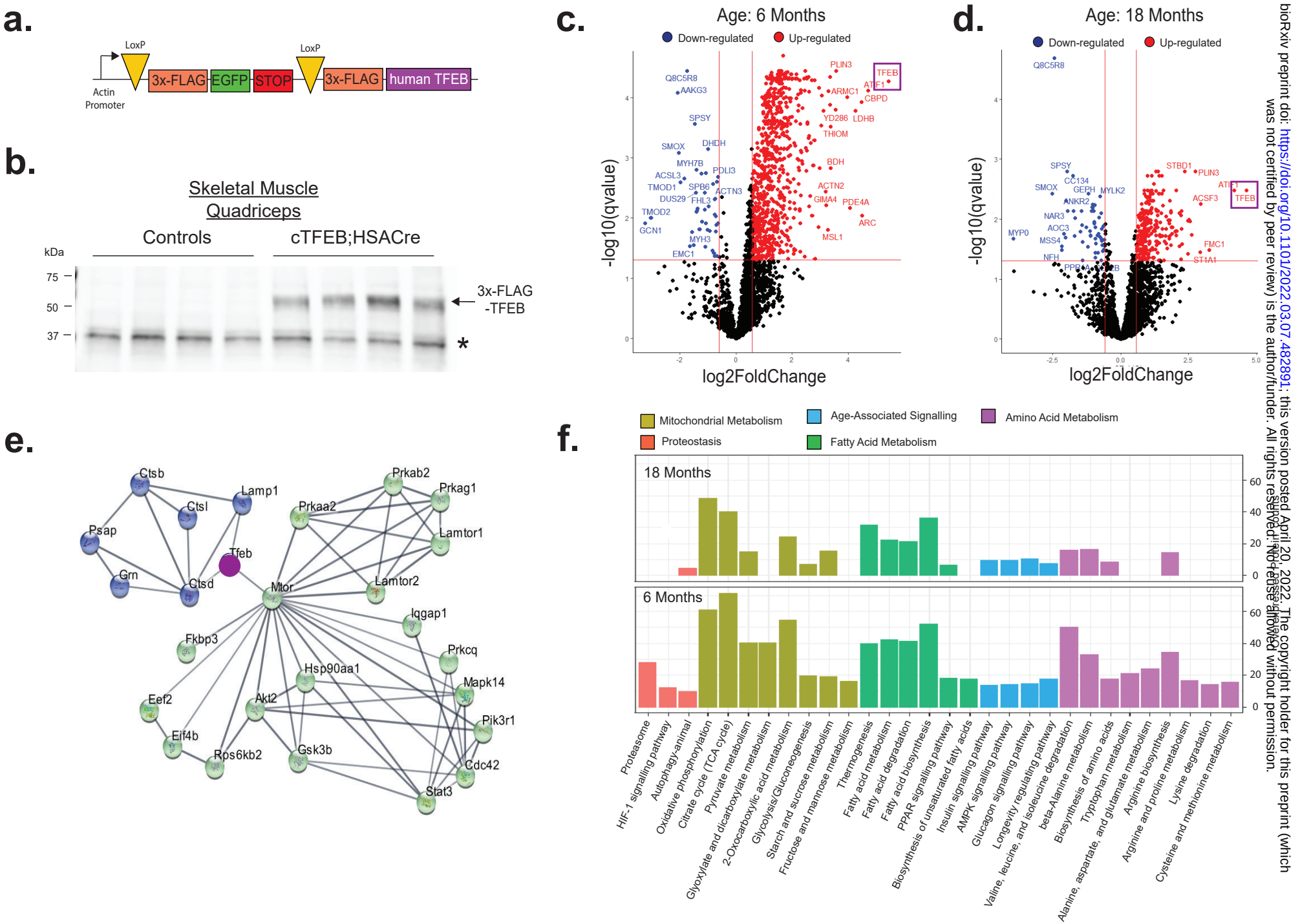

Figure 1: Enhanced Proteostasis Preserves Mitochondrial Function and Amino Acid Metabolism in Aging Skeletal Muscle. (a) Schematic depicting 3x-FLAG-human TFEB transgene. Cassettes are arranged from 5' (left) to 3' (right), with the β-actin promoter with CMV enhancer on the far 5' end, and a 3x-FLAG-eGFP STOP cassette flanked by loxP sites just 5' from the 3x-FLAG-human TFEB transgene. (b) Immunoblot of skeletal muscle lysates shows 3x-FLAG-TFEB expression (arrow) only in cTFEB;HSACre samples. Asterisk shows non-specific band demonstrating similar protein loading across samples (n=4 females/genotype, age: 6 months). (c-d) Proteomics analysis shows volcano plots of differentially expressed proteins in young (6 months) and aged (18 months) cTFEB;HSACre relative to control skeletal muscle (n=4 males/genotype/age). Each dot is a differentially expressed protein. Red dots are overrepresented proteins with TFEB-overexpression, and blue dots are proteins underrepresented with TFEB overexpression ($p<0.05$). Proteins that were not differentially expressed are shown in black (e) STRING analysis of overexpressed proteins in young TFEB-expressing skeletal muscle showing lysosomal network (in blue) and metabolic/aging network (in green). TFEB central node is shown in purple (f) KEGG enrichment analysis of differentially expressed proteins show significant enrichment for pathways known to modulate the biology of aging in cTFEB;HSACre transgenic mice. Enrichment of these pathways is mostly preserved in aged skeletal muscle.

Figure 2

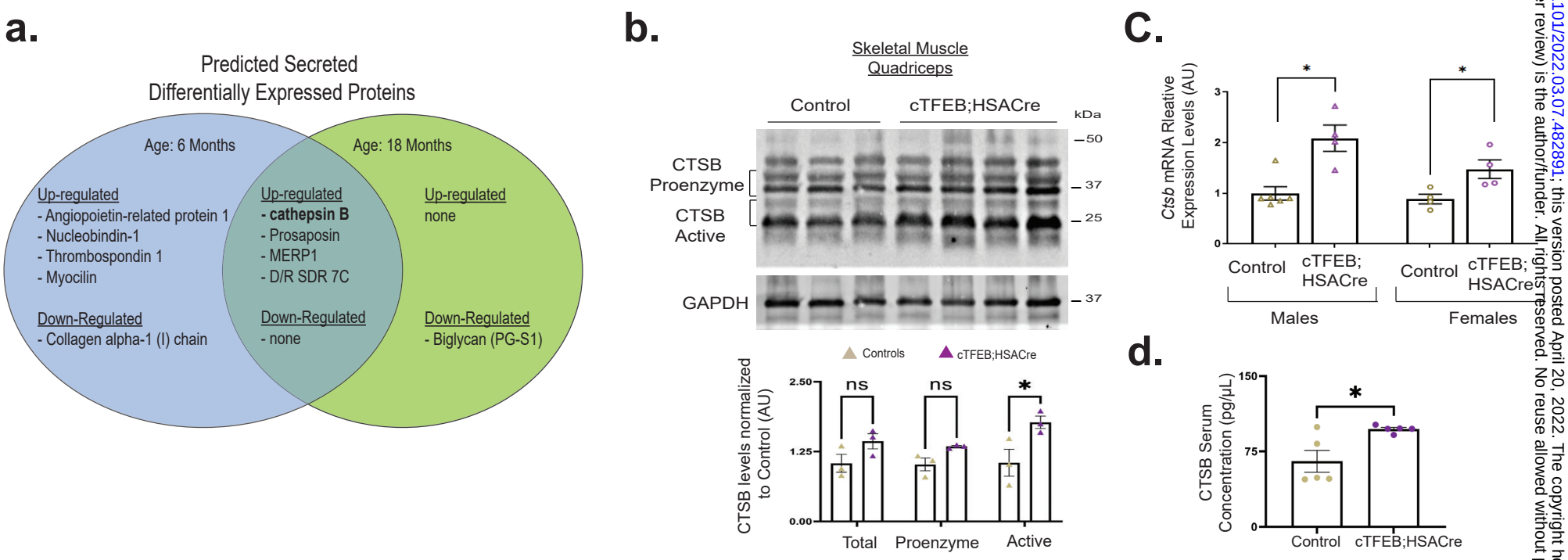

Figure 2: Increased Expression and Secretion of Cathepsin B from Skeletal Muscle with Enhanced Proteostasis. (a) VerSeDa-predicted secreted proteins identified as differentially expressed by proteomics studies in young (blue) and aged (green) cTFEB;HSACre mice. **(b)** Immunoblot analysis of cathepsin B protein. Note that the smaller, mature fragment of Cathepsin B is the secreted form (relative expression of total CTSB: controls: 1.04 ± 0.15 and cTFEB;HSACre: 1.43 ± 0.13, relative expression of pro-enzyme CTSB: controls 1.02 ± 0.11 and cTFEB;HSACre: 1.34 ± 0.02, relative expression of mature CTSB: controls 1.05 ± 0.24 and cTFEB;HSACre: 1.77 ± 0.11, n=3-4 males/genotype, age; 6 months). **(c)** Increased expression of *Ctsb* in TFEB expressing skeletal muscle (relative expression of controls: 1± 0.20 and cTFEB;HSACre: 4.91 ± 1.01), n=3-6 sex/genotype, age: 6 months). Elevated levels of cathepsin B in serum from cTFEB;HSACre mice (controls: 65.26 ± 10.87 pg/µl and cTFEB;HSACre: 97.26 ± 1.64 pg/µl) n=5-6 females/genotype, age; 6 months). Data are represented as mean± SEM * $p<0.05$, ** $p<0.01$, T-test.

Figure 3

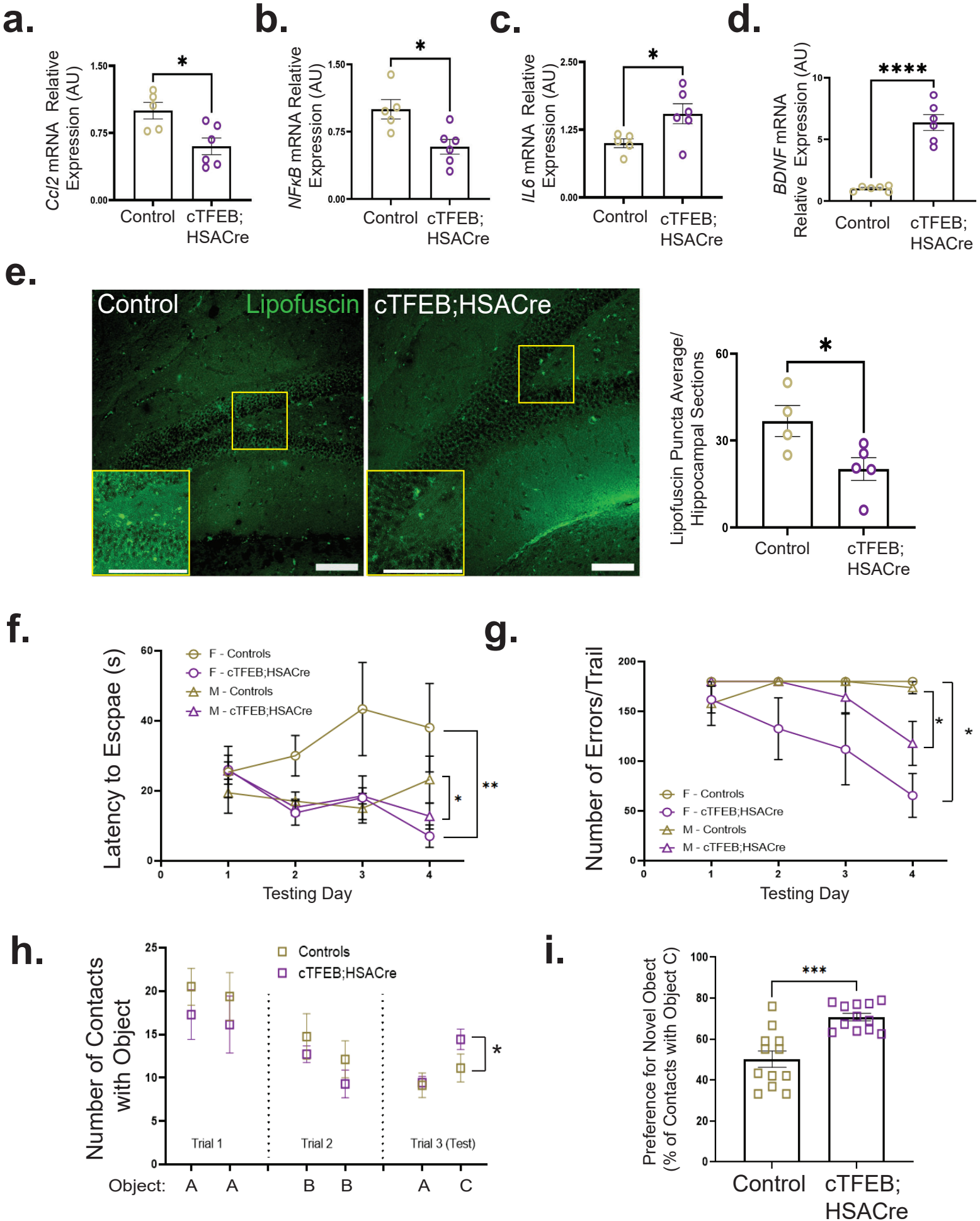

Figure 3: Skeletal Muscle Expression of TFEB decreases Neuroinflammation, Lipofuscin Accumulation, and Improves Cognitive Performance in Aged Mice. qRT-PCR of hippocampal lysates show decreased expression of *Ccl2* (relative expression of controls: 1 ± 0.11 and cTFEB;HSACre 0.60 ± 0.09) **(a)** and *NfκB* (relative expression of controls: 1 ± 0.11 and cTFEB;HSACre 0.58 ± 0.082) **(b)**, and increased expression of *Il6* (relative expression of controls: 1 ± 0.08 and cTFEB;HSACre 1.54 ± 0.18) **(c)** was detected in cTFEB;HSACre mice (n=6 females/genotype, age: 18 months) **(d)** Increased relative expression of BDNF in hippocampal lysates of cTFEB;HSACre mice relative to age-matched control littermates (controls: 1.02 ± 0.09 vs. cTFEB;HSACre 6.36 ± 1.59, n=6 females/genotype, age: 18 months) **(e)** Decreased accumulation of auto-fluorescent punctae (lipofuscin) in the dentate gyrus of the hippocampus of cTFEB;HSACre mice (average number of lipofuscin deposits/section/individual of controls: 36.75 ± 5.37 and of cTFEB;HSACre: 20.2 ± 3.92, n=4-5 females/genotype, age: 18 months). Each data point represents the average counts of 2-5 intact hippocampal sections/individual. Scale bars = 100 μm. Data are represented as mean± SEM * $p<0.05$, ** $p<0.01$, *** $p<0.001$ T-test. (**f-i**) Neurocognitive battery of 18 month old cTFEB;HSACre and control animals. cTFEB;HSACre mice escaped the Barnes maze more quickly (at day 4, control males 23.2 ± 6.67 vs cTFEB;HSACre males 12.8 ± 2.85 seconds to escape, control females 34.7 ± 7.2 vs cTFEB;HSACre females 6.6 ± 1.78 seconds to escape) **(f)** and made significantly less errors (at day 4, control males 173.9 ± 6.13 vs cTFEB;HSACre males 117.0 ± 22.14 errors, control females 180 ± 1.2 vs cTFEB;HSACre females 65.45 ± 22.02 errors) **(g)** than their littermate controls (2-way ANOVA, Alpha =0.05 ($F(1, 28) = 7.553$, $P=0.0104$), post-hoc T-test. Additionally, cTFEB;HSACre mice made significantly more contacts **(i)** (controls: 11.13 ± 1.6 vs. cTFEB;HSACre: 14.43 ± 1.18 contacts with novel object) and displayed a higher preference with **(i)** (controls: 50.19 ± 13.72 vs. cTFEB;HSACre: 70.78 ± 1.85% preference for novel object) the novel object than their age-matched control littermates (2-way ANOVA, Alpha =0.05 ($F(11, 33) = 2.534$, $P=0.0192$), post-hoc Kruskall-wallis-test. Data are represented as mean ± SEM * $p<0.05$, ** $p<0.01$.

Figure 4

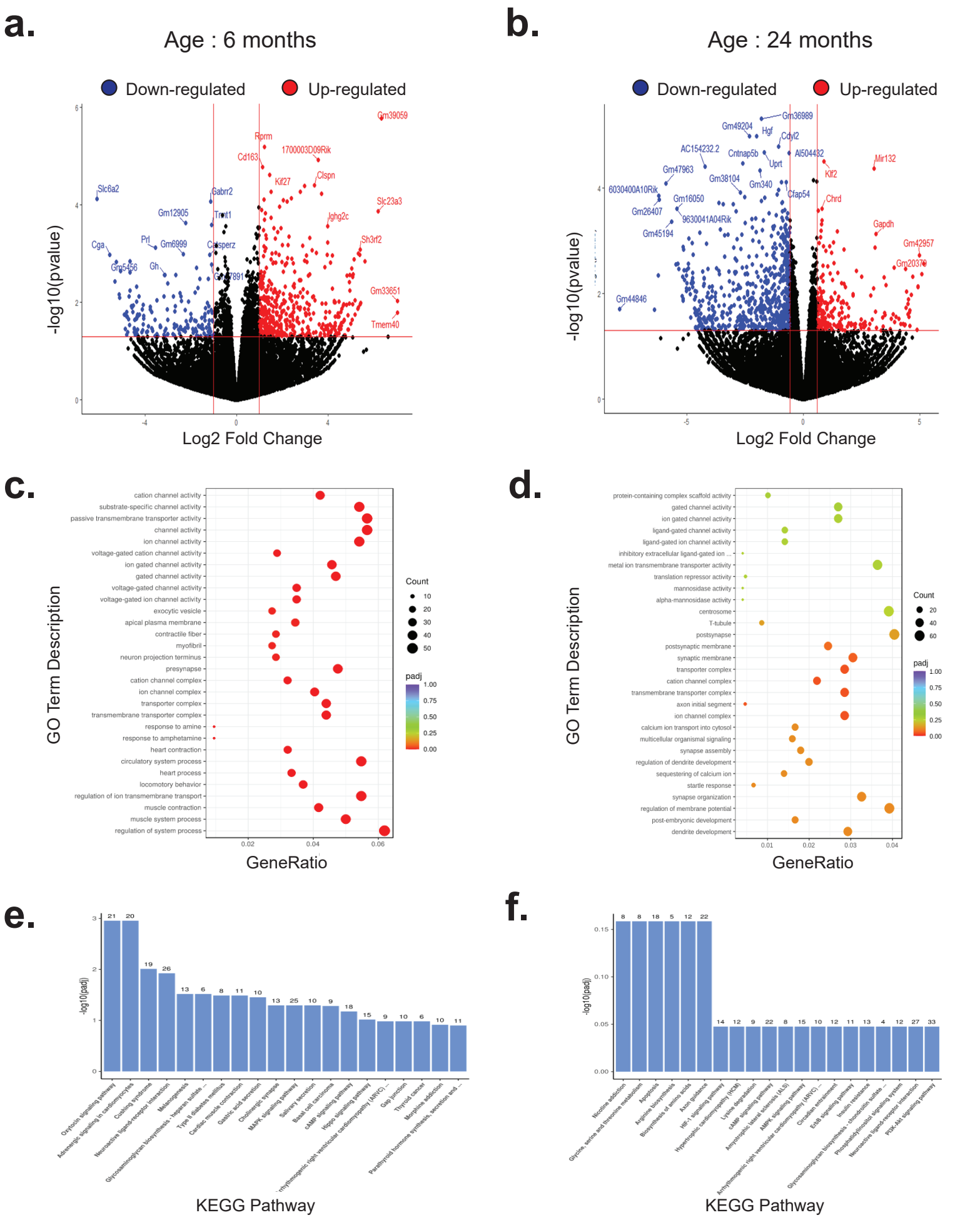

Figure 4: Hippocampal Transcriptomic Remodeling Associated with Synaptic Function and Cognitive Performance in Female cTFEB;HSACre Transgenic Mice. RNA-Seq of total hippocampal lysates showing differentially expressed transcripts in the hippocampi of young **(a)** and aged ($p<0.05$) **(b)** female cTFEB;HSACre mice (n=4 females/age/genotype, age: 6 months (young) and 24 months (aged). **(c-d)** GO term analysis of differentially expressed genes in the hippocampi of young female cTFEB;HSACre mice. **(e-f)** KEGG pathway enrichment of differentially expressed transcripts in the CNS of young and aged cTFEB;HSACre transgenic mice.

Figure 5

a.

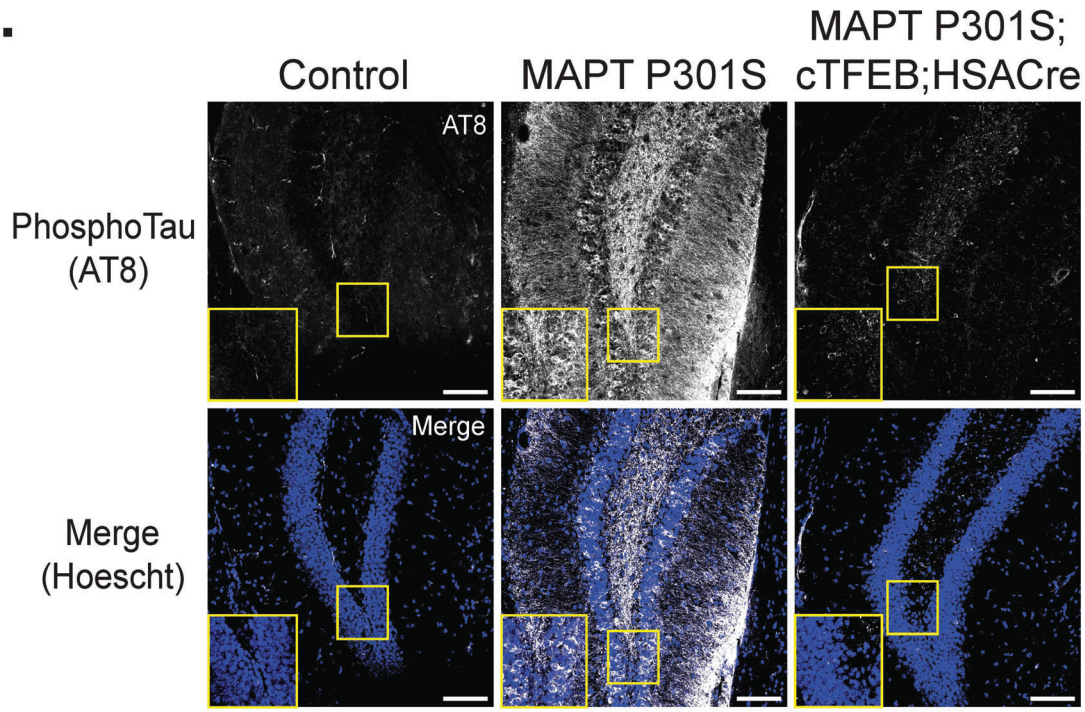

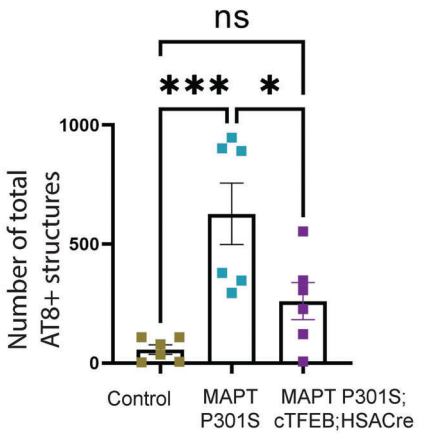

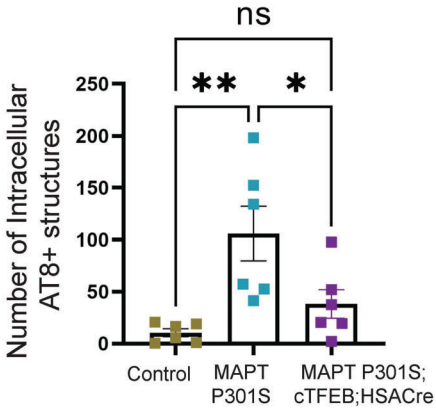

b.

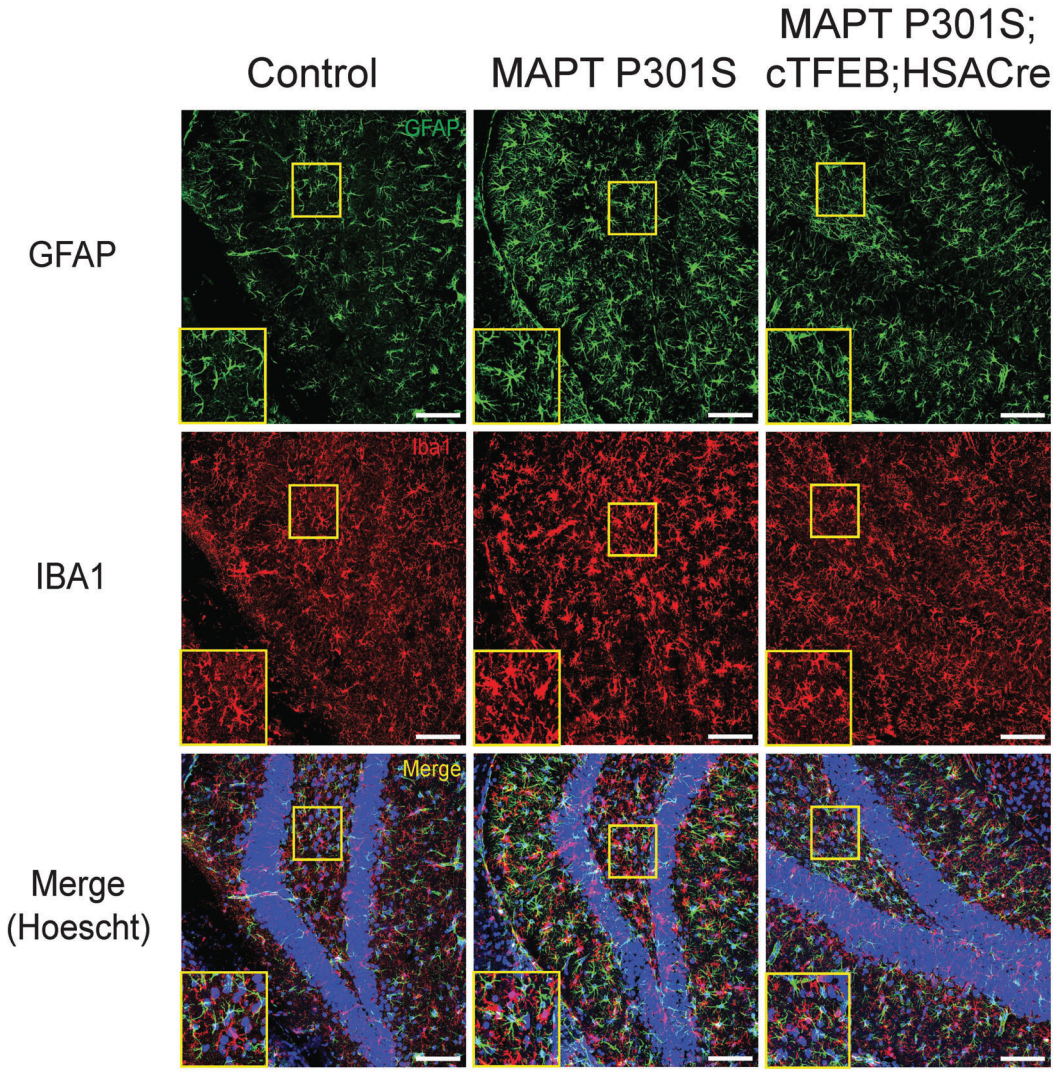

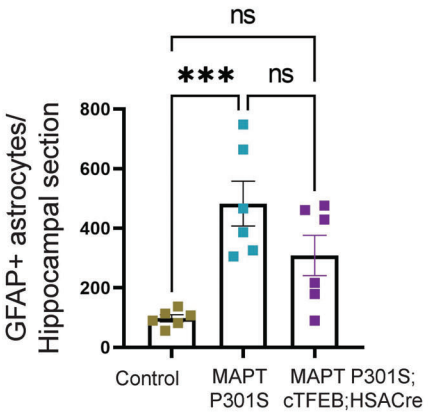

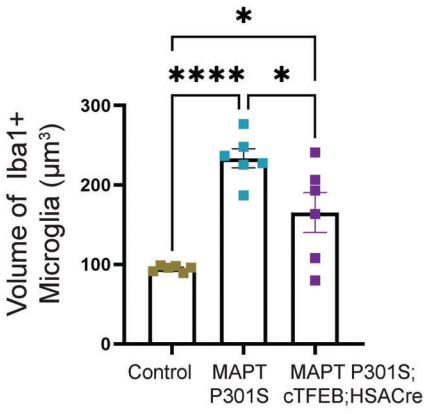

Figure 5: Enhanced skeletal muscle proteostasis rescues Pathogenic Tau Accumulation and Reduces Neuroinflammation in a Mouse Model of Tau pathology. (a) Immunohistochemistry depicting PhosphoTau staining (white) and Hoescht staining (blue) in the hippocampal dentate gyrus of Control (top) MAPT P301S (middle), and triple transgenic MAPT P301S;cTFEB;HSACre mice (bottom). Insets depicting intracellular PTau are 5X zooms of areas demarcated by yellow squares. Scale bars = 100 μm. Quantification of total Phosphotau tangles/section for both sexes of the three genotypes (mean of AT8+ structures in controls: 57 ± 19.87, MAPT P301S: 626.4 ± 129, MAPT P301S;cTFEB;HSACre: 257.2 ± 77.42) (right) and for intracellular Phosphotau tangles (Phosphotau staining overlapping with at least one pixel of Hoescht, mean of controls: 10.56 ± 3.79, MAPT P301S 105.0 ± 26.32, MAPT P301S;cTFEB;HSACre: 38.17 ± 13.80). Each data point represents the average counts of 2-5 intact hippocampal sections/individual (n=6, 3 males and 3 females/genotype, age: 9 months). **(b)** Immunohistochemistry of GFAP (green), IBA1 (red), and Hoescht (blue) staining in the dentate gyrus of Control (top) MAPT P301S (middle), and triple transgenic MAPT P301S;cTFEB;HSACre mice (bottom). Insets depicting glia morphology are 5X zooms of areas demarcated by yellow squares. Scale bars = 100 μm. Quantification for GFAP object number per section and process complexity (top right. Controls: mean number of astrocytes 97.56 ± 11.54, MAPT P301S mean number of astrocytes 482.7 ± 75.09 and MAPT P301S;cTFEB;HSACre mean number of astrocytes 308.5 ± 68) and IBA1+ microglia volume and process complexity (bottom right. Controls: mean volume of microglia 94.76 ± 1.61, MAPT P301S mean volume of microglia 233.6 ± 12.06 and MAPT P301S;cTFEB;HSACre mean volume of microglia 165.2 ± 25.06) for male and female mice of the three genotypes (n=6, 3 males and 3 females/genotype, age: 9 months). Each data point represents the average counts of 2-5 intact hippocampal sections/individual. Data are represented as mean± SEM * $p<0.05$, ** $p<0.01$, *** $p<0.001$, One-way ANOVA, post-hoc T-test.

Figure 6

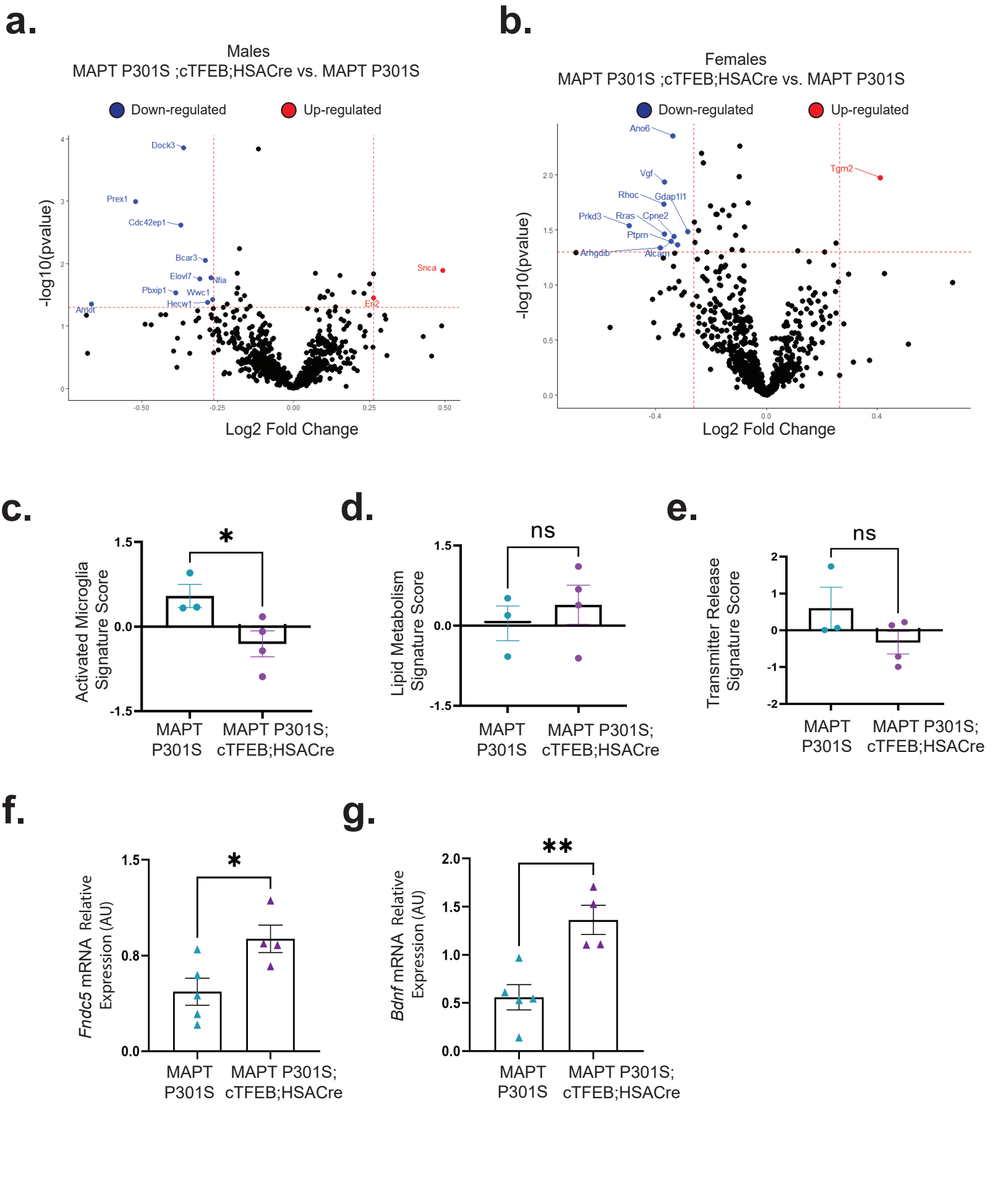

Figure 6: Increased Neurotrophic signaling and Modulation of AD-associated gene expression in MAPT P301S Transgenic Mice with Enhanced Skeletal Muscle Proteostasis

(a-b) Transcriptional expression of differentially regulated genes in the hippocampi of MAPT P301S;cTFEB;HSACre animals relative to age-matched MAPT P301S littermates ($p<0.05$). **(c)** Genes associated with microglial activation in the nCounter AD panel are downregulated in MAPT P301S;cTFEB;HSACre (score: -0.31 ± 0.23) compared to MAPT P301S age-matched littermates (score: 0.54 ± 0.21). **(d-e)** Differential up-regulation of lipid metabolism (MAPT P301S score: 0.04 ± 0.3 vs. MAPT P301S;cTFEB;HSACre score 0.39 ± 0.36) and down-regulation of transmitter release (MAPT P301S score: 0.60 ± 0.56 vs. MAPT P301S;cTFEB;HSACre score -0.34 ± 0.30) in MAPT P301S transgenic mice with enhanced skeletal muscle proteostasis. Analysis done via nSolver (Nanostring) differential gene expression analysis software. qRT-PCR of 9 month old female hippocampal lysates from the three aforementioned genotypes shows Increased relative expression of BDNF (MAPT P301S: 0.56 ± 0.13 vs. MAPT P301S;cTFEB;HSACre 1.34 ± 0.15, normalized to wild-type controls =1) **(f)** and FNDC5 (MAPT P301S: 0.46 ± 0.11 vs. MAPT P301S;cTFEB;HSACre 0.88 ± 0.11, normalized to wild-type controls =1) **(g)** in MAPT P301S;cTFEB;HSACre mice relative to age-matched MAPT P301S littermates. Data are represented as mean± SEM * $p<0.05$, ** $p<0.01$, T-test.